Chapter 3
KAWs in Magnetosphere-Ionosphere Coupling

3.1 Solar Wind-Magnetosphere-Ionosphere Interaction

Besides the sun shines on the earth there is an invisible direct interaction between the sun and the earth, that is the impact of the solar wind on the earth. The conception of intermittent plasma streams consisting of electrons and ions from the sun was introduced by Chapman and Ferraro (1930) to explain the cause of geomagnetic storms, and later the existence of the solar wind continuously blowing away from the sun was proposed successively by Biermann (1948, 1954, 1957) and Alfvén (1957) in their studies on comet tails to explain the deviation of the comet tail direction from the solar-comet radial direction (i.e., the solar radiation pressure direction) found by Hoffmeister in 1943. The theoretical model of the solar wind was presented by Parker (1958) and subsequently was confirmed by in situ measurement of the Explorer 10 satellite (Heppner et al. 1962; Bridge et al. 1962; Bonetti et al. 1963). Now it is generally known that the solar wind is a supersonic plasma stream with a very high Mach number of $M \sim 10$, which consists of electrons, protons, and ionized helium and minor other heavy ions as well as interplanetary magnetic fields originating from the sun and flows continuously at a high velocity ~300–800 km/s from the solar outermost atmosphere, that is, the solar corona.

The earth's magnetosphere, which is propped up by the earth's intrinsic dipolar magnetic field with a roughly north-south orientation, forms a huge umbrella to protect our living environment from the direct impinging of the solar wind plasma flow and other cosmic energetic charged particles. In fact, because of the interaction of the high velocity magnetized plasma flow of the solar wind with the geomagnetic field, the magnetosphere is compressed to $\sim 10 R_E$ on the dayside and to $\sim 20 R_E$ on the flank. While on the nightside the magnetosphere is stretched out into a long magnetotail extending beyond $\sim 10^3 R_E$. In result, the upper boundary of the magnetosphere, called the magnetopause, is shaped by the solar wind into a windsock, inside which a large magnetic cavity is carved out by the geomagnetic field in the solar wind, called the magnetosphere first named by Gold (1959). Since entering the space age,

D.-J. Wu and L. Chen, *Kinetic Alfvén Waves in Laboratory, Space, and Astrophysical Plasmas*, Atmosphere, Earth, Ocean & Space,
https://doi.org/10.1007/978-981-13-7989-5_3

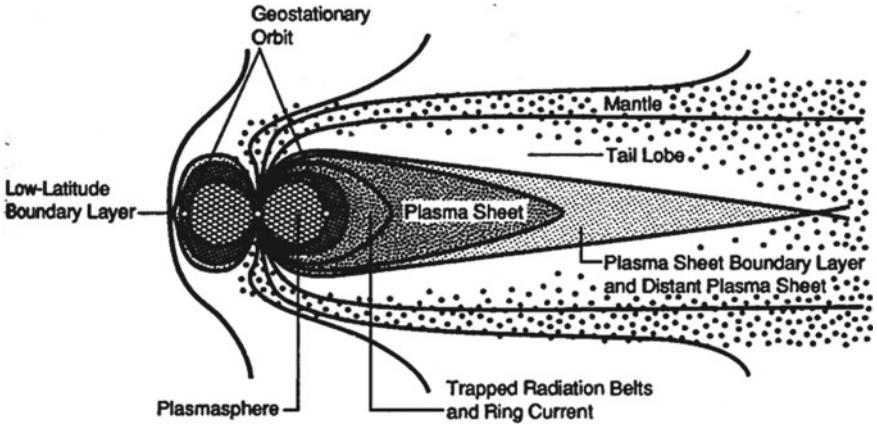

Fig. 3.1 A sketch of the magnetospheric structure as viewed in the noon-midnight meridian plane (from Wolf 1995)

a large number of in situ observations by satellites show that the magnetosphere is a fascinating mixture repository of complex plasma components and electromagnetic waves, including various complex plasma regions, such as the plasmasphere, the van Allen radiation belt, low latitude boundary layer (LLBL), high latitude boundary layer (HLBL, also called plasma mantle), central plasma sheet (CPS, also called plasma sheet), plasma sheet boundary layer (PSBL), plasma tail lobes, and so on. Figure 3.1 shows a sketch of the magnetospheric structure, in which some major plasma regions are briefly introduced below.

The plasmasphere, ranging from ∼1000 km above the ground to a geocentric distance $\sim 6R_E$ (or i.e., $\sim 5R_E$ above the ground), is one of the major regions of the magnetosphere, in which plasmas have typical density of $n \sim 10^3$ cm^{-3} and temperature of $T \sim 1$ eV. These dense and cold plasmas are believed to come from so-called the "polar wind" originating from the upper-ionosphere, where the plasma has a temperature close to the gravitational binding energy (Banks and Holzer 1969). The plasma density of the plasmashphere has a sharp decrease at a boundary layer at altitudes of ~ 3–$5R_E$, called the "plasmapause". Besides these dense cold plasmas from the ionosphere, however, a large number of energetic particles, as tenuous and hot components, also coexist in approximately this region, that is, so-called the van Allen radiation belts of mainly consisting of energetic particles trapped in the magnetic field of the magnetosphere. These energetic particles have energies typically ranging from keV to MeV and there is a peak at around ∼100 keV in the energy spectrum of the ions. Below 10 keV, O^+ is the dominant ion, but H^+ begins to dominate above 50 keV. In particular, these energetic ions contribute the majority of the ring current, in which about half of the ring current is contributed by ions below 85 keV and other half by ions above 85 keV. In addition, energetic electrons inside the radiation belts contribute relatively little to the ring current as well as the total energy of trapped particles. Moreover, unlike the case of energetic ions, the radial

distribution of the flux of energetic electrons above 1 MeV has one obvious "slot" centered about $\sim 2.2 R_E$, that is, a minimum in fluxes, and the inner and outer parts of this slot are called the "inner radiation belt" and "outer radiation belt", respectively.

On the other hand, the magnetotail on the nightside consists of three major regions. One is the north and south tail lobes between the plasma mantle (i.e., the HLBL) and the PSBL, in which there are open magnetic fields and low-density cold plasma originating from the ionosphere (density below 0.1 cm^{-3}, energy below 1 keV). The CPS is located on the outer side of the nightside plasmasphere and consists of hot plasmas (of keV energies) with densities typically ~ 0.1–$1\ cm^{-3}$. In the CPS the magnetic fields are closed mostly, although sometimes there are some closed loops of magnetic flux, called "plasmoids", that do not connect to the earth or solar wind. Observations show that the CPS ion population is a mixture of ionospheric and solar wind particles (being mostly of solar-wind origin in quiet times and mostly ionospheric in active times) and has the temperature about several times of the electron temperature and flow velocities much less than the ion thermal velocity. The PSBL is a transition region between the almost empty tail lobes and the hot CPS, in which ions with densities of the order of 0.1 cm^{-3} typically exhibit flow parallel or antiparallel to the local magnetic field at velocities of hundreds of km/s, higher than their thermal velocity. Thus, counterstreaming ion beams of propagating earthward and tailward along the local magnetic field can be observed frequently in the PSBL. In particular, the counterstreams tend to be unstable to various plasma waves. Therefore, various plasma waves and wave-particle interactions are very essential and ubiquitous kinetic processes in collisionless magnetospheric plasmas.

The lower boundary of the magnetosphere is the ionosphere at an altitude range $\sim$100 to $\sim$1000 km above the ground. The existence of the ionosphere, as an electrically conducting layer of the upper atmosphere, was proposed early by Stewart in 1882 to be responsible for the solar-modulated variations of the geomagnetic field that was postulated by Gauss. Later in 1902 Kennely and Heaviside suggested that this conducting layer, initially known as the Kennely-Heaviside layer, is able to reflect radio waves and hence may explain the Marconi radio experiment on transatlantic radio transmissions between England and Canada in 1901. The existence of the ionosphere, however, was verified first by Appleton and Barnett in the United Kingdom in 1924 and by Breit and Tuve in America in 1925 via the reflecting experiment of radio signals, later named the "ionosphere" by Watson-Watt and Appleton in 1926 (see Chian and Kamide 2007). Subsequently, Chapman (1931a, b) developed a theory of upper atmospheric ionization to explain the formation of the ionosphere and its structuring into layers that were found by Appleton, in which, the ionosphere, as a by-product of the sun-earth interaction, is produced mainly via the photoionization by the solar radiation in the ultraviolet and extreme ultraviolet bands. Therefore, the ionosphere consists of dense, collisional, and partially ionized plasmas and acts as a transition layer from the fully ionized magnetospheric plasma to the neutral atmosphere on the ground. In particular, the ionosphere can absorb the major energy of high-energy photons from the solar radiation as well as of energetic particles from cosmic rays, solar energetic particles, and magnetospheric hot particles. Of course, these energetic particles also may lead to the ionosphere ionization via the impact

ionization. The ionization in the ionosphere increases with the altitude and the plasma density reaches its peak $n_e \sim 10^5$ to 10^6 cm^{-3} at the altitude of ∼250 km.

The electrodynamics of the solar wind-magnetosphere-ionosphere interaction can be described by the so-called global current system, which consists of main six types of large scale currents. One is the magnetopause boundary current flowing on the magnetopause, also called the "Chapman-Ferraro current", which consists of diamagnetic currents via the density and temperature across the boundary layer and was proposed first by Chapman and Ferraro (1930, 1931). The second is the ring current encircling the earth inside the magnetosphere, which is produced mainly by the magnetic gradient and curvature drift motions of energetic ions trapped in the radiation belt of the magnetosphere. The third is the tail current, which flows on the outer boundary of the magnetotail and around the tail lobes. The fourth is the neutral sheet current flowing in the transition region between the north and south tail lobes with nearly antiparallel magnetic fields. The fifth is the ionospheric currents consisting of the Pedersen current along the ionospheric induced electric fields but perpendicular to the magnetic fields and the Hall current perpendicular to both the electric and magnetic fields. The final is the field-aligned current flowing along the earth's magnetic field lines and connecting the magnetosphere to ionosphere, also called the "Birkeland current" or the "auroral current", which was found first by Birkeland (1908) when he analyzed his extensive data on the geomagnetic perturbations associated with auroras and concluded that large electric currents flowed along the local magnetic fields during aurora. A sketch of the global current system shown in Fig. 3.2, in which the ionospheric currents have not been displayed because their sizes are too small to appear. These currents interconnect to establish a global current system and their magnetic fields superpose the earth's intrinsic dipolar field to configure the dynamical magnetosphere.

When impinging on the dayside magnetosphere, a fraction of the solar wind energy flux enters the magnetosphere via magnetic reconnection or viscous-like processes (Akasofu 1981). The solar wind power penetrating the magnetosphere is $\sim 10^{10}$ to 10^{11} W during a quiet solar wind and $\sim 10^{12}$ to 10^{13} W during a strongly disturbed solar wind, which may be caused by an interplanetary coronal mass ejection originating from solar eruptive activity. Although the solar wind power input into the magnetosphere is much less than the radiation power received at earth from the solar shining, known as the solar constant, $\simeq 1.73 \times 10^{17}$ W, it can play an important and crucial role in the dynamics of the magnetosphere.

The solar wind energy entering the magnetosphere, via the global current system, is firstly transferred and distributed, intermediately stored, and eventually released and dissipated in somewhere in the system. For example, some of the energy entering the dayside magnetosphere is directly transferred to the high-latitude ionosphere via field-aligned currents and is dissipated by the ionospheric Joule heating. The remainder is transferred to the magnetotail and stored into the magnetotail current system. Then, one part of the energy stored in the magnetotail is transferred to the ring current where it is dissipated mainly via the charge exchange with neutrals into the atmosphere, another part is transferred to the auroral ionosphere via the field-aligned currents where it is dissipated into auroral radiations and plasma heating, and the

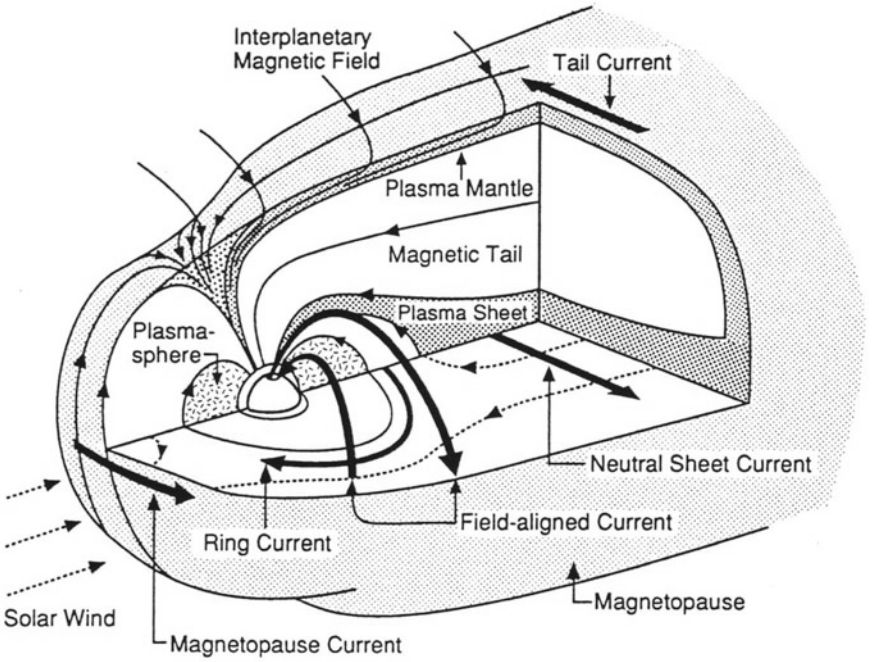

Fig. 3.2 A sketch of the global current system (from Russell 1995)

rest is not dissipated inside the magnetosphere but is released into the downstream solar wind via the down-tail plasmoids in the magnetotail.

When the energy transferring rate from the solar wind into the magnetosphere is low, the magnetosphere responds to these energy processes in a quasi-steady manner, that is, the geomagnetic quiet state. When the energy input rate is relatively high, however, the magnetosphere reacts in a non stationary or explosive manner, such as geomagnetic storms and substorms. Accompanying the electrodynamical processes of the global current system during these storms and substorms, various plasma waves and their wave-particle interactions must appear ubiquitously in the magnetosphere and ionosphere, in particular in the current channels of the global current system, such as the magnetopause, magnetotail, boundary layers, and field-aligned current channels. These current-channel areas have the characteristic mesoscales that typically are much smaller than the macroscales of the global large-scale structures but much larger than the microscales of the particle kinetics. These mesoscale structures can supply plentiful free energy that drives various microscale processes, such as the excitation of various plasma waves and corresponding wave-particle interactions. These microscale waves and wave-particle interaction play essentially and crucially important roles in the energy transport and dissipation of the global current system as well as the energization and diffusion of magnetospheric and ionospheric particles.

In order to comprehensively understand the dynamics of the global current system and its response to the solar wind fluctuations, in principle, it is necessary to consider the solar wind-magnetosphere-ionosphere coupling system as a whole. Because of the complexity and difficulty of the total system, however, current researches basically focus on a few key links of the coupling system, such as the solar wind-magnetosphere coupling in the magnetopause and the magnetotail and the magnetosphere-ionosphere coupling in the polar magnetosphere and auroral plasmas. Therefore, they have been the main objects of satellite exploration since the space age. In particular, a large number of in situ observations by satellites in space plasmas show that KAWs can play a crucially and essentially important role in these key regions of the coupling system. In this chapter we focus on the observation and application of KAWs in the auroral plasma dynamics, especially their application in the auroral electron acceleration, and the next Chap. 4 will discuss KAWs in the solar wind-magnetosphere coupling, with particular emphasis on their application in the transport and heating of plasma particles.

3.2 Aurora and Magnetosphere-Ionosphere Coupling

The aurora, a beautiful and mysterious phenomenon in the Earth's atmosphere, consists of lights in the sky that are emitted by atoms and molecules in the upper atmosphere at the altitude of $\sim$100 km, where neutral gases are ionized and excited by collisions with energetic electrons, called auroral energetic electrons, precipitating from the magnetosphere into the atmosphere. It is most commonly seen in the latitude of $\sim 20^\circ$ from the geomagnetic poles and in the form of auroral arcs, luminous curtains stretching over hundreds of km along the east-west direction, but very much thinner in the north-south extent with a few of km. The microphysics of acceleration of these auroral energetic electrons has long been an open problem. Although it is possible that energetic electrons from the sun are guided directly into the polar region by the geomagnetic field, these energetic electrons can not be responsible for producing auroras because they have neither sufficient energy to produce the magnificent optical displays nor do they strike the atmosphere in the proper locations.

The generation mechanism of auroras, especially the acceleration mechanism of the auroral energetic electrons has been studied over several decades by many ground-based observations as well as by sounding rocket and satellite in situ measurements. These observations have revealed that the auroral phenomena are associated with energetic electrons of 1–10 keV that have relations with enhancements of the upward field-aligned currents during substorms (Mcllwain 1960; Mozer et al. 1980). The tendency that there are higher fluxes of the energetic electrons at smaller pitch angles implies that their acceleration is dominated by the field-aligned acceleration processes (Hoffman and Evans 1968). The energy distribution of these auroral energetic electrons is characterized by a precipitous decrease above 10 keV, without a rapid increase towards energies below 4 keV (Bryant 1990). Figure 3.3 presents a typical example of energy distributions of observed auroral energetic electrons

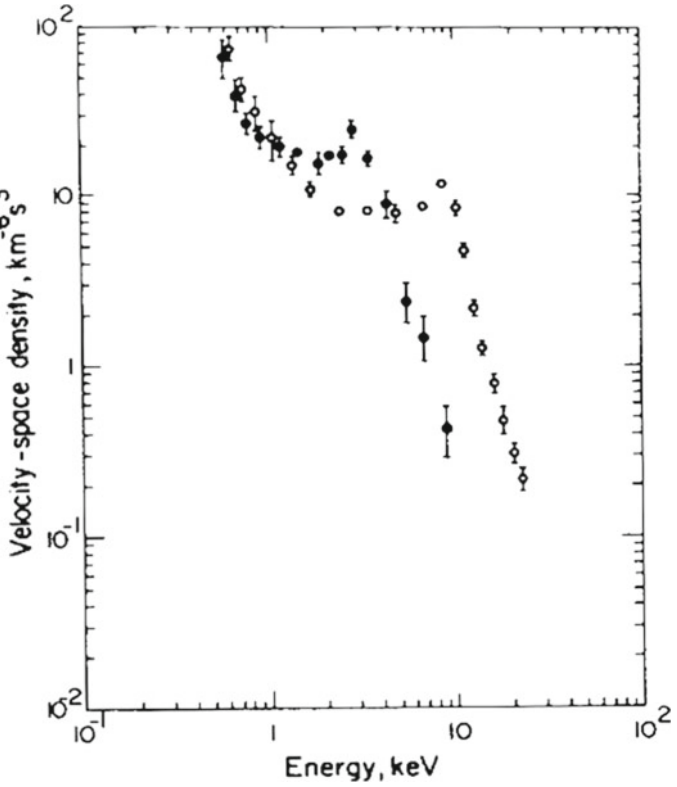

Fig. 3.3 Typical electron energy distributions which are responsible for discrete aurora. The measurements were obtained at the centre (open circles) and edge (solid circles) of an auroral arc with a Skylark rocket, SL 1422, launched from Andoya Norway on 21 Nov. 1976 (from Bryant 1981)

(Bryant 1981), where the open and solid circles give the electron energy distributions measured at the centre and edge of the observed auroral arc. From Fig. 3.3 the auroral energetic electrons of the edge have a similar distribution feature to that of the center but lower energies than that of the center.

In particular, the comparison between the energy distributions of field-aligned electrons simultaneously measured by the DE-1 and 2 satellites in the higher magnetospheric altitude ($\sim 2R_E$) and the lower ionospheric altitude ($\sim 0.1R_E$) clearly demonstrates that the acceleration of auroral energetic electrons occurs in the region of altitudes of a few to ten thousands of km (or i.e., ~ 0.5–$2R_E$), called the auroral acceleration region (Reiff et al. 1988). This indicates that the auroral electron acceleration strongly depends on the environmental condition of the ambient plasma and occurs only in some specific locations in the polar magnetosphere with not only specific latitudes corresponding to the auroral zone but also specific altitudes corresponding to the auroral acceleration region, as well as at specific times corresponding to the duration of substorms.

In fact, besides beautiful and visible auroras these auroral energetic electrons have a mysterious product, that is, so-called auroral kilometric radiation (AKR, Gurnett 1974). AKR is produced by the electron cyclotron maser emission of the auroral energetic electrons at the local electron cyclotron frequency and/or its harmonic frequency (Wu and Lee 1979; Lee and Wu 1980). However, AKR had no been found until space observations onboard satellites became available in 1960s because its frequencies are below the cutoff frequency (i.e., ω_{pe}) of the ionosphere and hence can not enter into the atmosphere and arrive on the ground.

Based on the analysis results of a large number of in situ measurements of the auroral plasma in various altitudes from the low ionosphere ($\sim 10^2$ km) to the high magnetosphere ($\sim 10^5$ km), the auroral energetic electrons have the following main observed properties:

Field-aligned acceleration: The auroral energetic electrons are field-aligned accelerated by parallel electric fields and hence lead to intense field-aligned currents;

Characteristic energy: The auroral energetic electrons have typical energies of several keV and range from 1 to 10 keV;

High-energy cutoff: The auroral energetic electrons have energy spectra characterized by downward extending to the thermal distribution of the background electrons and upward precipitously decreasing above 10 keV;

Acceleration region: The auroral acceleration region is located in the range of altitudes a few to ten thousands of km (or i.e., ~ 0.5–$2R_E$), which also is the source region of AKR and has very dilute plasma density so that $\omega_{pe} \ll \omega_{ce}$;

Discrete auroral arc: Discrete auroral arc produced by the auroral energetic electrons of precipitating to the ionosphere has a typical width $\sim$ a few km, and the electrons in the auroral arc edges have a similar energy spectrum with that in the auroral arc center but lower energies.

The magnetosphere and ionosphere are strongly coupled by the geomagnetic field and the field-aligned current along the field lines in the Earth's polar region, where the auroral plasma with variable parameters in the magnetosphere and ionosphere directly is vertically penetrated by the geomagnetic field. In particular, the rapidly precipitating auroral energetic electrons must lead to sharply increasing of the field-aligned current and a series of corresponding electrodynamical responses of the polar magnetospheric plasma, also called the auroral plasma, and the visible aurorae is only their response in the ionosphere. Therefore, the auroral plasma dynamics is the base to understand the substorm and auroral phenomena. From the low ionosphere ($\sim 10^2$ km) to the high magnetosphere ($\sim 10^5$ km), however, the magnetosphere-ionosphere coupling system contains a rich variety of plasma populations with the density varying from 10^6 cm^{-3} to less than 10^{-2} cm^{-3}, the temperature from lower than 1 eV to higher than 100 keV, and the magnetic field from 0.5 G to 50 nT with the altitude increasing. It is evident that the altitude distribution feature of the plasma parameters can play an important role in the magnetosphere-ionosphere coupling. Although vast measurements for these polar plasmas have been carried out by ground-based observations and sounding rocket and satellite in situ explorations,

it still is very difficult to describe perfectly variations of these plasma parameters with altitudes.

Based on in situ measured data, the plasma density can be calculated by the ion density or by the electron density. In principle, the ion and electron densities should be same because of the charge neutrality condition. The ion components in the auroral plasma consist mainly of oxygen (O^+) and hydrogen (H^+). The oxygen ions originate from the ionosphere and behave at lower altitudes according to the barometric exponent law (Thompson and Lysak 1996), that is,

$$n_O = n_{IO} \exp\left(-h/h_O\right), \tag{3.1}$$

where n_{IO} is the oxygen density in the ionosphere, h is altitude in units of R_E, and h_O is the oxygen scale height (usually a few % of R_E). The hydrogen ions (i.e., protons) originate in the upper ionosphere and magnetosphere and their behavior follows an exospheric power law (Thompson and Lysak 1996),

$$n_H = n_{IH} \left(1 + h\right)^{-m}, \tag{3.2}$$

where n_{IH} is the hydrogen density in the ionosphere and the index m is typically between 1 and 3.

According to the charge neutrality condition, the electron density profile can be modeled by the combination of Eqs. (3.1) and (3.2). Combining the altitudinal density profile measured by the S3-3 satellite in the auroral acceleration region (Mozer et al. 1979) with an exponentially decreasing ionospheric component, Lysak and Hudson (1987) suggested a function to model the distribution of the ambient electron density along the auroral field lines as follows:

$$n(r) = n_0 \exp\left(-\frac{r - r_0}{h_0}\right) + \frac{17\ \mathrm{cm}^{-3}}{(r-1)^{1.5}}, \tag{3.3}$$

where $r = 1 + h$ is the geocentric distance in units of R_E. In this expression, the first term represents the ionospheric density component which can be fitted by density measurements made during a rocket flight and the second term comes from the fitting density determined by the measurements recorded on the S3-3 satellite in the evening auroral zone (Lysak and Hudson 1979). A further comparing with a composite of electron density measurements made by Viking, DE 1, ISIS 1 and Allouette II, Kletzing and Torbert (1994) showed that the modeled profile and the in situ measurements can agree quite well when $n_0 = 6 \times 10^4\ \mathrm{cm}^{-3}$, $r_0 = 1.05$, and $h_0 = 0.06$ in the altitude through $h = 0$ to 4 (R_E) above the ionosphere.

Based on the above analyses of the ion and electron densities, following Kletzing and Torbert (1994), Wu and Chao (2004) takes the ambient plasma density of the auroral plasma, n, as

$$n(h) = 1.38 \times 10^5 \exp\left(-\frac{h}{0.06}\right) + 17h^{-m}\ (\mathrm{cm}^{-3}), \tag{3.4}$$

where m is a fitting parameter used to fit the magnetospheric plasma density and the charge neutrality condition of $n_e = n_i = n$ has been assumed for the ambient plasma density.

For the distribution of the ambient auroral plasma temperature with the altitude, it is generally believed that the magnetospheric temperature is remarkably higher than the ionospheric temperature and that the plasma temperature can change from below 1 eV in the ionosphere up to a few hundreds of eV in the magnetosphere at altitudes of $h \sim 3$–$4R_E$, where the plasma is dominated by the plasma sheet with temperature of ~300–600 eV. Based on measurements of temperature up to the highest altitudes measured by S3-3, Kletzing et al. (1998, 2003) showed that the temperature commonly is below 10 eV at altitudes below 10,000 km ($h \sim 1.5R_E$) and the majority of the measurements gives a temperature lower than 5 eV at altitudes below $1R_E$. Therefore, they inferred that the temperature may begin to increase slightly with the altitude at 7000 km due to the effect of a decline in the cold ionospheric density relative to the hotter CPS component (Kletzing et al. 1998). Taking the magnetospheric temperature as ~300 eV, the temperature profile described by Kletzing et al. (1998) can be modeled by the following formula (Wu and Chao 2004)

$$T_e = 100\,[1 + \tanh\,(h - 2.5)]^{3/2}\ \text{(eV)}. \tag{3.5}$$

Unlike the cases of the ambient density and temperature, the ambient magnetic field in the auroral plasma is relatively simple and clear and can be modeled well, at least within a few Earth's radii, by the variation of the Earth's dipolar field as follows:

$$B_0 = \frac{0.6}{(1+h)^3}\ \text{(G)}. \tag{3.6}$$

Figure 3.4 plots the distributions of the ambient plasma parameters with the altitude (h) above the ionosphere, where panels, from the top down, are the electron density n_e (a) in Eq. (3.4) with the fitting parameter $m = 1.5$, temperature T_e (b) in Eq. (3.5), the magnetic field B_0 (c) in Eq. (3.6), the Alfvén velocity v_A (d), and the electron thermal to Alfvén velocity ratio $\alpha_e = v_{T_e}/v_A$ (e), respectively. In the calculation of the Alfvén velocity, the ion mass density of the auroral plasma, ρ_m, is obtained by the sum of oxygen ($16n_{O^+}m_p$) and hydrogen ($n_{H^+}m_p$) ions, that is,

$$\rho_m = 2.208 \times 10^6 e^{-h/0.06} + 17h^{-m}\ (m_p/\text{cm}^3), \tag{3.7}$$

where m_p is the proton mass.

Figure 3.4d, e show clearly that the auroral plasma has a high Alfvén velocity of $v_A > 10^4$ km/s and hence a low electron thermal to Alfvén velocity ratio of $\alpha_e < 1$, especially in the auroral acceleration region, which is located at the altitude ~0.5–$2R_E$, one has $\alpha_e \ll 1$ and $v_A \sim 0.1c$. One of key and difficult problems in understanding the physics of the auroral electron acceleration is how to produce and maintain a large parallel electric field that can accelerate field-aligned electrons to keV-order energies (Fälthammar 2004). In general, the very large parallel

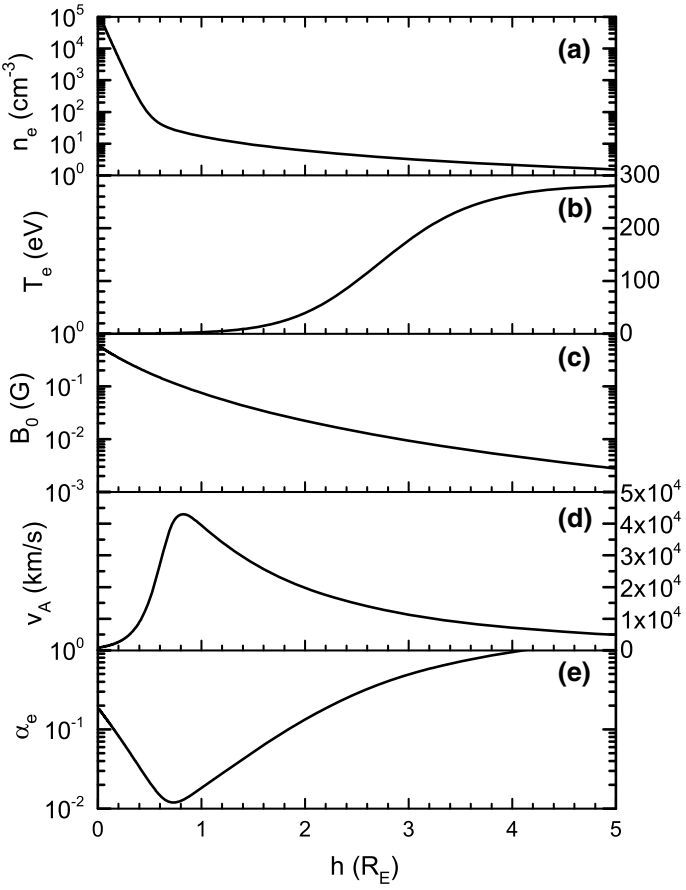

Fig. 3.4 The ambient plasma parameter distributions with the altitude above the ionosphere h (R_E): **a** The electron density n_e in cm^{-3}; **b** the electron temperature T_e in eV; **c** the Earth's magnetic field B_0 in G; **d** the Alfvén velocity v_A in km/s; and **e** the electron thermal to Alfvén velocity ratio $\alpha_e \equiv v_{T_e}/v_A$

conductivity can immediately short-circuit any parallel electric fields in a collisionless plasma such as in the magnetosphere. Many "non-ideal" mechanisms, e.g., the "anomalous resistivity" concept (Papadopoulos 1977), the "weak double layer" model (Temerin et al. 1982; Boström et al. 1988; Mölkki et al. 1993), and the direct acceleration by lower-hybrid waves (Bingham et al. 1984) had been invoked as possible explanations.

Wu and Chao (2004) proposed that solitary KAWs (SKAWs) can play an important role in the auroral energetic electrons, in which effective parallel electric fields can be maintained by the inertial motion of electrons. Since 1990s, solitary structures of strong electric field fluctuations have been commonly observed by in situ measurements of the polar-orbit satellites, such as the Freja, FAST and Polar satellites, in

the polar ionospheric and magnetospheric plasmas and are identified well as SKAWs (Louarn et al. 1994; Wu et al. 1996a, b, 1997; Chaston et al. 1999). Moreover, the satellite observations also show that the strong KAWs, SKAWs or turbulent KAWs, in the auroral plasma are often associated with the field-aligned acceleration of electrons as well as the cross-field heating of ions (Stasiewicz et al. 2000a). Following, we first introduce the observation and identification of SKAWs in the auroral plasma in Sect. 3.3 and then discuss their theoretical models in Sect. 3.4.

3.3 Observation and Identification of SKAWs

In 1980s, possible applications of KAWs in the formation of discrete auroral arcs had been discussed by some authors (Hasegawa 1976; Goertz and Boswell 1979; Goertz 1981, 1984; Lysak and Dum 1983). However, there were little high resolution in situ measurements that can directly and clearly identify out the fine structures associated with small-scale KAWs. An important example is the identification of electromagnetic fluctuations with a two-dimensional vortex structure (Chmyrev et al. 1988). By the data from the Intercosmos-Bulgaria-1300 satellite (ICB-1300), which measurements of electric and magnetic fields have higher temporal resolution than the previous satellite measurements, Chmyrev et al. (1988) analyzed some strong magnetic and electric field fluctuations on short temporal scales, which occurred on both the polar and equatorial edge of the auroral oval. The measured magnetic fluctuations with $\delta B_{\parallel} \ll \delta B_{\perp}$ and the electric to magnetic fluctuation ratio of $\delta E_{\perp}/\delta B_{\perp} \sim v_A$ indicate these fluctuations to be incompressible Alfvénic modes. In particular, they found, by use of hodograms of the electric field that the perturbed fields have two-dimensional vortex structures and identified them as drift-KAWs. Moreover, the electron flux within the "vortex" region exceeds the background by 2 orders of magnitude, implying that the electrons are trapped within the Alfvénic vortex and travel together with it, from the generation region in the magnetosphere to the observation region in the ionosphere. The authors proposed that the measured drift-KAWs can be directly associated with the structures of auroral arcs. Similar vortex structures associated with KAWs were measured more clearly and refinedly in the laboratory experiments of the LAPD (Burke et al. 2000a, b). The more refined and evident in situ measurement and identification of fine structures associated with KAWs in space plasmas were achieved in following space explorations by the polar-orbit satellites, Freja and FAST, which had the higher temporal resolution to resolve smaller scale structures.

The Freja satellite, a joint Swedish and German scientific satellite, was launched on October 6, 1992 in Jiuquan, China, into a polar orbit traversed the auroral oval almost tangentially in the East-West direction, with 63° inclination and an apogee of 1750 km and perigee of 600 km (see Lundin et al. 1994 for more details). In the auroral plasma environment explored by Freja, the electron density and temperature have a typical value $n_e \sim 10^3$ cm^{-3} and $T_e \sim 1$ eV, respectively, and the geomagnetic field $B_0 \simeq 0.2$ G at the Freja altitude. This indicates the explored low-β plasma

($\beta \sim 10^{-6} \ll Q$) with the electron inertial length $\lambda_e \sim 100$ m and the ion-acoustic gyroradius $\rho_s \sim 10$ m, which are the characteristic scales of KAWs. KAWs have frequencies below the ion gyrofrequency $\omega_{ci}/2\pi \sim$ a few 100 Hz for hydrogen ions or $\sim$ a few 10 Hz for oxygen ions in the Freja exploring environment. The Freja satellite is designed for fine-structure plasma measurements with a high temporal/spatial resolution of the auroral plasma processes. Its experiments allowed three-dimensional measurements of direct-current (at 128 Hz sampling rate) and alternating-current (at 32 kHz sampling rate) magnetic fields with a set of fluxgate and search coil magnetometers. Similarly, two dimensional direct-current (at 768 Hz sampling rate) and alternating-current (at 32 kHz sampling rate) electric fields are measured by a set of probe pairs 7.6–21 m apart from each other. These measurements provided, together with the sampling rate of 32–64 ms resolution electron distribution functions, excellent means of observing the microphysics of KAWs in the auroral plasma environment explored by the Freja satellite.

By use of the data from Freja, Louarn et al. (1994) found that the low-frequency electromagnetic fluctuations with frequencies ~1–20 Hz lower than the local ion gyrofrequency, consist of two distinct kinds. One is the widespread distributed electromagnetic turbulence (typically tens mV/m in the electric fluctuation and tens nT in the magnetic fluctuation) associated with a lower level of the density fluctuation ($|dn/n| \lesssim 10\%$). The other is the solitary strong electric spikes lasting tens ms, which typically have a stronger electric fluctuation ($\delta E \sim$ hundreds mV/m) by one order of magnitude and a similar magnetic fluctuation ($\delta B \sim$ tens nT), and are associated with a strong density fluctuation ($|dn/n| \sim$ tens percent). Two typical examples of them are shown in Fig. 3.5, where panels, from the top down, are electric field, magnetic field, and density fluctuations, respectively. The durations of these two structures both are well below 0.1 s but above 0.05 s, implying their fluctuation frequencies ~10–20 Hz. The event on the left panel has the electric field amplitude ~0.6 V/m, magnetic amplitude ~40 nT, and relative density amplitude ~80%. Other one on the right panel is relative weaker and has the electric field amplitude ~0.2 V/m, magnetic field amplitude ~15 nT, and relative density amplitude ~30%.

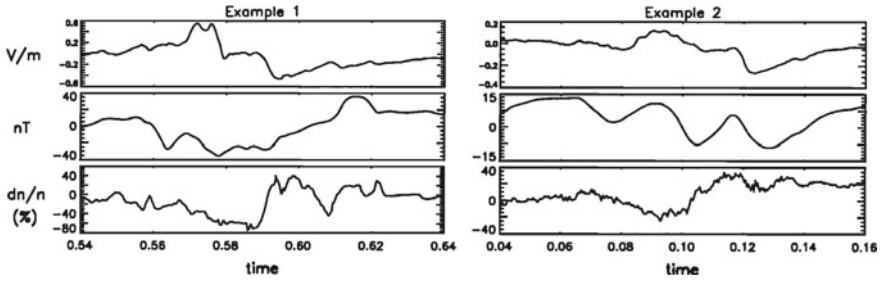

Fig. 3.5 Two examples of SKAWs observed by the Freja satellite during passing the auroral zone at the altitude ~1700 km above the ionosphere on 09/03/1993 (from Louarn et al. 1994)

Louarn et al. (1994) analyzed in detail the electromagnetic features and accompanying density fluctuations of these strong electric spikes and found that their electric to magnetic fluctuation ratio $\delta E/\delta B \sim 5 \times 10^6$ m/s $\sim v_A$ (the local Alfvén velocity), which is the typical characteristic of Alfvénic fluctuations, that is, nonlinear AWs. Their accompanying deep density cavities (i.e., density dips), however, imply that their structures must have been significantly modified by some kinetic effects. Moreover, their short duration of tens ms corresponds a cross-field size of hundreds m, i.e., a few times the local electron inertial length, which is the typically perpendicular wavelength of KAWs in the inertial regime of $\alpha_e < 1$. These clear characteristics of inertial-regime KAWs lead to the conclusion that these solitary strong electric spikes are the nonlinear structures of inertial-regime solitary KAWs (SKAWs, Louarn et al. 1994).

Wu et al. (1996b) further found that these strong electric spikes are accompanied not only by density dips but also often by density humps. According to the theory of one-dimensional SKAWs, inertial-regime SKAWs with $\alpha_e < 1$ are accompanied by only density dip soliton (Shukla et al. 1982), while kinetic-regime SKAWs with $\alpha_e > 1$ are accompanied by only density hump soliton (Hasegawa and Mima 1976). In order to explain the Freja observation of SKAWs accompanied by hump as well as dip solitons, the initial conjecture by Wu et al. (1996b) is that the Freja satellite was traversing the plasma transition region between kinetic and inertial regimes. A more serious conflict between the observation and theory, however, was found soon after by Wu et al. (1996a, 1997). They analyzed some strong density fluctuations ($|dn/n| > 10\%$) accompanying SKAWs observed by the Freja satellite and found that these SKAWs can be accompanied by not only single dip or hump structures, but also composite structures of dip and hump, called the "dipole density soliton".

Two typical examples of the dipole density soliton are shown in Fig. 3.6, their dipole density amplitudes are the dip -50% and hump $+55\%$ for the left one and the dip -40% and hump $+55\%$ for the right one. Table 3.1 lists 21 dipole density solitons accompanying SKAWs (including the two examples at 0935:25.80 and 0935:56.65 shown in Fig. 3.4) presented by Wu et al. (1996a, 1997), which were observed by the Freja satellite when it crossed the auroral plasma at the altitude about 1700 km on days 3 March 1993, 9 March 1993, and 7 March 1994. In Table 3.1, the "time" column lists the universal time (UT) of events, the "dn/n" column presents their

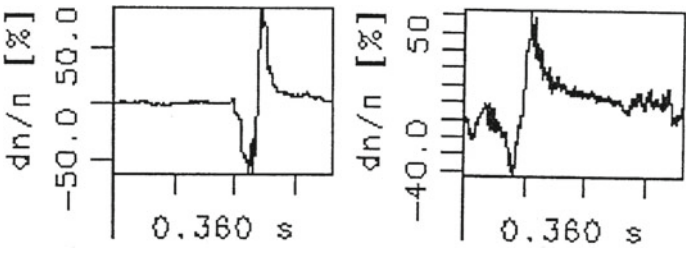

Fig. 3.6 Two examples of dipole density soliton observed by the Freja satellite (from Wu 2010)

Table 3.1 Density solitons associated with the Freja SKAW events (reprinted the table with permission from Wu et al., Phys. Rev. Lett. 77, 4346, 1996a, copyright 1996 by the American Physical Society)

Time (UT)	$dn/n(\%)$	Δt(ms)	Solitons	Time (UT)	$dn/n(\%)$	Δt(ms)	Solitons
0935:16.80	−30(+40)	80	Dipole	0935:53.70	−70	50	Dip
0935:25.80	−50(+70)	70	Dipole	1702:06.95	−30	40	Dip
0935:36.65	−40(+45)	90	Dipole	1703:30.90	−50	50	Dip
0935:54.80	−15(+20)	80	Dipole	1703:33.00	−50	80	Dip
0935:56.85	−40(+15)	80	Dipole	1703:34.85	−30	50	Dip
1703:18.85	−35(+20)	90	Dipole	2039:10.70	−20	60	Dip
1703:52.85	−55(+50)	90	Dipole	1659:03.10	+40	70	Hump
1704:50.85	−20(+15)	70	Dipole	1703:08.80	+60	60	Hump
1704:52.85	−40(+25)	90	Dipole	1704:51.10	+15	40	Hump
0344:59.15	−75(+40)	60	Dipole	2034:03.00	+20	50	Hump
0348:05.60	−25(+35)	60	Dipole				

density amplitudes with the sign "−" or "+" denoting the density "dip" or "hump", respectively, the "Δt" column gives the durations of the SKAWs, and the "solitons" column is the types of density solitons.

From Table 3.1, it can be found that the dipole density solitons are more frequently present than single dip or hump solitons. The number of dipole solitons (11) is about one-half of the total number of SKAWs, and the number of single dip solitons (6) or single hump solitons (4) is about one-fourth of the total number of SKAWs. Moreover, the dipole density solitons have, in average, a larger spatial scale than single dip or hump solitons by a factor of 1.6. The dipole solitons have a typical duration ∼80 ms, corresponding the spatial size scale ∼560 m and the typical duration of the single dip or hump solitons ∼50 ms, corresponding the spatial size scale ∼350 m, estimated by the Freja satellite velocity ∼7 km/s.

Since the three types of density solitons (dip, hump, and dipole) all are associated with similar local electromagnetic fluctuations with the KAW characteristics, that is, associated with SKAWs, and also all take place in the same plasma environment, that is, the auroral plasma at the altitude ∼1700 km, they should be uniformly described by the same physical model. Wu et al. (1996a, 1997) generalized the theory of SKAWs from the one-dimensional case to the two-dimensional case and found that the two-dimensional SKAW model with a dipole vortex structure can uniformly explain well not only the presence of the three kinds of density solitons (i.e., dip, hump, and dipole solitons) but also the rotation character of electric fields associated with the observed SKAWs (Chmyrev et al. 1988; Volwerk et al. 1996).

Volwerk et al. (1996) further analyzed the electromagnetic character of these SKAWs in the Freja observations and their carrying Poynting flux. They found that these strong electromagnetic spikes ($\delta E \sim$ hundreds mV/m and $\delta B \sim$ tens nT) have mainly a rotational character in the plane perpendicular to the geomagnetic field

and a tiny magnetic compressional component not exceeding 4% in general. Therefore, they came to the conclusion that these SKAWs are two-dimensional structures associated with small-scale ($\sim$ hundreds m) tubular currents. In addition, they also found that the Poynting flux carried by these SKAWs along the geomagnetic field is typically in the order of $\sim$0.05–0.1 mW/m^2. In both intensity and direction the Poynting flux of these SKAWs is comparable to the typical value required by the auroral acceleration electrons. In particular, their analysis shows that these SKAWs are situated at the edge of large-scale shear regions in the current, where the plasma density appears obviously the inhomogeneity, as observed in the LAPD experiments (Burke et al. 2000a, b).

Other polar-orbit satellite launched soon later, the FAST (Fast Auroral SnapshoT) satellite, also presents similar observation results of SKAWs. The FAST satellite was launched on August 21, 1996 into an 83° inclination polar orbit with 350 km perigee and 4180 km apogee (Carlson et al. 1998) and was designed for studying the microphysics of fine-scale Alfvénic fluctuations observed in the auroral oval. It provides not only three-dimensional electromagnetic field measurements but also multiple baseline electric field measurements thereby removing the temporal/spatial ambiguity inherent in single point measurements and providing direct evidence of the observed spatial structures of KAWs with a perpendicular drift smaller than the satellite velocity. KAWs in the electron inertial length size are observed by the FAST satellite from perigee at 350 km up to apogee at 4180 km. Their observed properties further confirm the observations made by Freja. However, the FAST's high inclination orbit provides a different perspective with a generally north-south cut (rather than east-west) through the flux tubes on which these waves exist. Furthermore, the eccentricity of the orbit allows an altitude profile for these waves to be established extending from just above the ionosphere to the base of the primary auroral electron acceleration potential.

Figure 3.7 shows the transverse electric to magnetic field ratios and the perpendicular sizes of over 100 SKAWs observed by the FAST satellite in similar altitudes (1500–2500 km), where the panel (a) plots the transverse electric to magnetic field ratio versus the local Alfvén velocity and the panel (b) gives the distribution of the perpendicular size of SKAWs in units of the electron inertial length (Chaston et al. 1999). The results show that these SKAWs are characterized typically by: (1) strong electric spikes ($\delta E \sim$ hundreds of mV/m) and magnetic pulses ($\delta B \sim$ tens of nT), which yield the electric-magnetic amplitude ratio, $\delta E/\delta B$, of a few times the local Alfvén velocity, as expected by the theory of the inertial-regime SKAWs (see Sect. 3.4); (2) short durations of tens ms implying a frequency much lower than the local ion gyrofrequency $\sim$ a few hundreds Hz and a transverse scale $\sim$ hundreds of m, which averages to several times the local electron inertial length and is the typical scale of the inertial-regime SKAWs (see Sect. 3.4); (3) accompanying strong density perturbations $\sim$ tens percent. These results are completely similar with that from the Freja observations of SKAWs and confirm again the conclusion that the observed strong electromagnetic spikes are inertial-regime SKAWs.

In fact, the strong electromagnetic spikes (hundreds mV/m electric field fluctuations and tens nT magnetic field fluctuations), accompanying strong density fluctu-

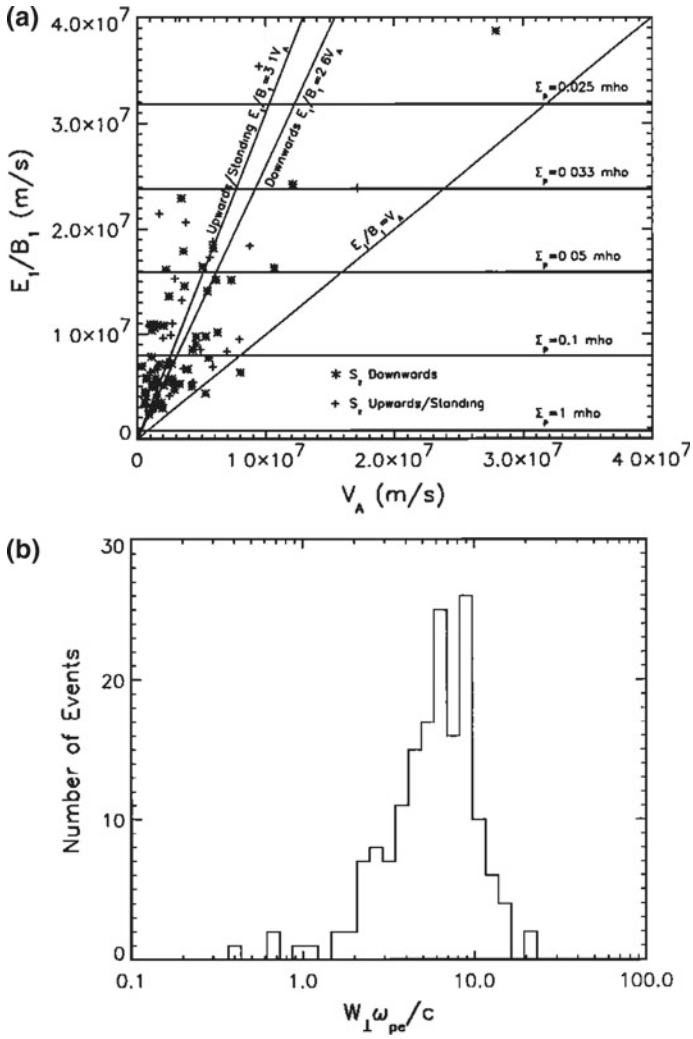

Fig. 3.7 Properties of SKAWs observed by the FAST satellite: **a** the distribution of the transverse electric to magnetic field ratio versus the local Alfvén velocity; **b** the distribution of the perpendicular size of SKAWs in units of the electron inertial length (from Chaston et al. 1999)

ations (tens percent) are very common features in the observations of the Freja and FAST satellites when they cross the auroral plasma at the altitudes ∼1000–4000 km (Louarn et al. 1994; Wahlund et al. 1994a; Volwerk et al. 1996; Wu et al. 1996a, b, 1997; Huang et al. 1997; Stasiewicz et al. 1997, 1998, 2000b, 2001; Bellan and Stasiewicz 1998; Chaston et al. 1999). Using novel plasma instruments and a high data rate, the two satellites provided a "first" high resolution plasma diagnostics that permit studies of meso- and micro-size scale phenomena in the 100-meter range

for plasma particles and in the 10-meter range for electric and magnetic fields. This provides adequate and reliable experimental data for the detailed studies in their physical property and the establishment of their theoretical models.

3.4 Theoretical Models of SKAWs in Auroral Plasmas

It is evident that the strong electromagnetic spikes, which accompany with strong density fluctuations and present commonly in the observations of the polar-orbit satellites, such as Freja and FAST, during passing through the auroral plasma, are solitary structures of nonlinear KAWs. A variety of nonlinear effects can occur frequently in a plasma because of strongly electromagnetic coupling interactions among charged particles. One of the most typical nonlinear effects is the steepening effect of dispersive waves, in which the wave front steepens and the amplitude enlarges when a fast wave chases and then overtakes a slow wave in a dispersive wavelet. Meanwhile, the dispersive effect in the wavelet also causes the waves to diffuse because of their different phase velocities. When the dispersive effect just balances the steepening effect, a localized and stationary coherent structure can be formed from the wavelet, which can stably propagate without changing its profile, called solitary wave, or soliton (Zabusky and Kruskal 1965).

In the case of KAWs, the existence of exact travelling wave solutions of SKAWs for the kinetic regime of $1 < \alpha_e^2 < Q^{-1}$ (or i.e., $Q < \beta/2 < 1$) was first demonstrated by Hasegawa and Mima (1976) and the corresponding kinetic-regime SKAWs are shown to be accompanied by a hump density soliton. While for the case of the inertial regime of $\alpha_e^2 < 1$ (or i.e., $\beta/2 < Q$) Shukla et al. (1982) also argued the existence of exact solution of SKAWs, but the corresponding inertial-regime SKAWs are accompanied by a dip density soliton. The first exact analytical solution of inertial-regime SKAWs with an arbitrary amplitude was obtained by Wu et al. (1995). In the small amplitude limit, preserving the lowest order nonlinearity, it leads to the standard KdV soliton, as expected.

Wu et al. (1996b) further extended the existence of SKAWs to the more general parametric regime, including the kinetic-inertial transition regime of $\alpha_e^2 \sim 1$. In particular, they presented the universal criterion for the existence of SKAWs (Wu et al. 1996b). In the low frequency approximation of $\omega \ll \omega_{ci}$, the density fluctuation of SKAWs, which correspond to nonlinear wavelets propagating at the direction of $\mathbf{k} = (k_x, 0, k_z)$, can be described by localized solutions (i.e., solitary wave solutions) of the following Sagdeev equation (Wu et al. 1996b):

$$\frac{1}{2}\left(\frac{dn}{d\eta}\right)^2 + K(n; M_z, k_x) = 0 \tag{3.8}$$

with the localized boundary conditions

$$n = 1; \quad v_{ez} = 0; \text{ and } d/d\eta = 0 \text{ for } \eta \to \pm\infty \tag{3.9}$$

in the traveling-wave (or i.e., co-moving) coordinates

$$\eta = k_x x + k_z z - \omega t, \tag{3.10}$$

where $K(n; M_z, k_x)$ is the so-called Sagdeev potential as follows:

$$K(n; M_z, k_x) = -\frac{(1+Q)\, M_z^2 n^4}{k_x^2 \left(M_z^2 - \alpha_e^2 n^2\right)^2} \times \left[\Phi_1 + \frac{\alpha_e^2}{M_z^2}\Phi_2 + \frac{1+\tau}{1+Q}\frac{Q\alpha_e^2}{M_z^2}\left(\Phi_3 + \frac{\alpha_e^2}{M_z^2}\Phi_4\right)\right] \tag{3.11}$$

with

$$\begin{aligned}
\Phi_1 &= \frac{(n-1)^2}{2}\left(M_z^2 - \frac{n+2}{3n}\right), \\
\Phi_2 &= n\,(1 - n + n\ln n) - M_z^2 n^2\,(n - 1 - \ln n)\,, \\
\Phi_3 &= \frac{(n-1)^2}{2} - M_z^2 n\,(1 - n + n\ln n)\,, \\
\Phi_4 &= M_z^2 n^2 \frac{(n-1)^2}{2} - n^2\,(n - 1 - \ln n)\,,
\end{aligned} \tag{3.12}$$

and $M_z \equiv M/k_z$ is the parallel phase speed in units of v_A. In these expressions, space x, y, z, time t, and density n are normalized by λ_e, $\lambda_e/v_A = \sqrt{Q}/\omega_{ci}$, and n_0, respectively, M is the phase speed in units of v_A, n_0 is the ambient plasma density.

In the expression (3.11) for the Sagdeev potential, the third term (associated with Φ_3 and Φ_4 and to be proportional to $Q\alpha_e^2 = \beta_e/2$) represents the so-called finite-β effect, which can be attributed to the coupling of the ion-acoustic wave with KAWs and is neglectable in low-β plasmas (Yu and Shukla 1978; Kalita and Kalita 1986; Wu and Wang 1996). While the first two terms, associated with Φ_1 and Φ_2, can be attributed to the inertial force and the kinetic pressure of electrons, respectively, and reduce to the inertial-regime case for $\alpha_e < 1$ (Shukla et al. 1982) and the kinetic-regime case for $\alpha_e > 1$ (Hasegawa and Mima 1976).

It is obvious that the necessary condition for a real solution of the Sagdeev equation (3.8) is the Sagdeev potential of Eq. (3.11) less than or equal to zero (i.e., $K(n; M_z, k_x) \le 0$). Thus, a variable range of the density n of the SKAW is determined by two adjacent roots of the Sagdeev potential $K(n; M_z, k_x) = 0$. One is $n = 1$, implying the ambient plasma density and other one should be the nearest by $n = 1$, assumed to be $n_m = n_m(M_z, \alpha_e)$, implying the amplitude of the density variation. Therefore, the so-called nonlinear dispersion relation that describes the relationship between the phase velocity M_z and the amplitude n_m can be obtained

from the condition $K(n; M_z, k_x) = 0$. For the case of low-β plasmas, neglecting the finite-β effect, the nonlinear dispersion relation for SKAWs can be given as follows:

$$M_z^2 = \left[\frac{n_m+2}{6n_m} + \alpha_e^2 n_m^2 \frac{n_m - 1 - \ln n_m}{(n_m-1)^2}\right] \pm \sqrt{\left[\frac{n_m+2}{6n_m} + \alpha_e^2 n_m^2 \frac{n_m - 1 - \ln n_m}{(n_m-1)^2}\right]^2 - 2\alpha_e^2 n_m \frac{1 - n_m + n_m \ln n_m}{(n_m-1)^2}}. \tag{3.13}$$

In the approximations of $\alpha_e^2 \ll 1$ and $\alpha_e^2 \gg 1$, this leads to the nonlinear dispersion relations

$$M_z^2 = \frac{n_m+2}{3n_m} \tag{3.14}$$

for inertial-regime SKAWs (Shukla et al. 1982) and

$$M_z^2 = \frac{1 - n_m + n_m \ln n_m}{n_m - 1 - \ln n_m} \frac{1}{n_m} \tag{3.15}$$

for kinetic-regime SKAWs (Hasegawa and Mima 1976), respectively.

It is especially worth noting the analogy between the Sagdeev equation (3.8) and the motion equation of a classical "particle" with the unit mass in the Sagdeev potential well where $K(n; M_z, k_x) \le 0$ between $n = 1$ and $n = n_m$, and η and n represent the "motion time" and the "spatial position" of the classical "particle", respectively. A soliton solution of Eq. (3.8) indicates the reciprocating motion of the "particle" constrained in the potential well between two points $n = 1$ and $n = n_m$, but with a period of infinity, that is, the "particle" moves only once back and forth between $n = 1$ and $n = n_m$, where n_m is the maximum (or minimum) of the density n in the soliton and determined by the nonlinear dispersion relation $K(n; M_z, k_x)|_{n=n_m \ne 1} = 0$. Based on this analogy, the necessary and sufficient conditions for the existence of the exact solutions for SKAWs can be stated as follows (Wu et al. 1996b):

1. $K(n) \le 0$ for $n \in [1,\ n_m]$;
2. $K(n) = 0$ at $n = 1$ and $n = n_m$;
3. $d_n K(n) = 0$ at $n = 1$ and $(n_m - 1)\, d_n K(n) > 0$ at $n = n_m$.

The condition (1) ensures that the Sagdeev equation (3.8) has a real solution and means that the "particle" moves in a constraining potential well between $n = 1$ and $n = n_m$. The condition (2) means that the "motion velocity" ($d_\eta n = \pm\sqrt{-2K(n)}$) of the "particle" reaches zero at both the two boundaries of the potential well at $n = 1$ and $n = n_m$, otherwise the "particle" does not move back and forth, but moves outside the potential well, implying a shock-like solution instead of a soliton. The condition (3) means that the "particle" is reflected back at the boundary of $n = n_m$ (i.e., the "acceleration" of the "particle" $d_\eta^2 n = -d_n K(n) \ne 0$ and with a direction from the

point $n = n_m$ to the point $n = 1$), but not reflected at the other boundary of $n = 1$ (i.e., the "acceleration" $d_\eta^2 n = 0$ at $n = 1$), otherwise the "particle" reciprocates with a finite period, that is, a periodically oscillational solution instead of a soliton solution. The combination of these three conditions gives the general criterion for the existence of the exact solutions for SKAWs.

In the small amplitude limit of $|N_m| \equiv |n_m - 1| \ll 1$, the nonlinear dispersion relation (3.13) reduces to $\delta M_z \equiv M_z - 1 = -N_m/3$, or i.e., $N_m = -3\delta M_z$. In particular, the Sagdeev equation (3.8) reduces to the standard soliton equation, that is, the KdV equation. The above condition (3) of the existent criterion for SKAWs leads to the inequality:

$$\delta M_z \left(1 - \alpha_e^2\right) > 0 \Rightarrow N_m \left(1 - \alpha_e^2\right) < 0, \tag{3.16}$$

implying that kinetic-regime SKAWs with $\alpha_e > 1$ are sub-Alfvénic ($\delta M_z < 0$) and accompanied by a hump ($N_m > 0$) soliton and inertial-regime SKAWs with $\alpha_e < 1$ are super-Alfvénic ($\delta M_z > 0$) and accompanied by a dip ($N_m < 0$) soliton.

From Fig. 3.4e, in the auroral plasma region between 0.2 and $1.8R_E$, which covers well the auroral acceleration region, we have $\alpha_e < 0.1$, implying in which the inertial-regime approximation can be satisfied well. In the inertial-regime approximation of $\alpha_e \ll 1$, an exactly analytical solution of the Sagdeev equation (3.8) can be obtained as follows:

$$N = N_m \frac{1 - \tanh^2 Y}{1 + N_m \tanh^2 Y}, \tag{3.17}$$

where

$$Y \equiv \frac{|\eta|}{k_x D} + \frac{N_m}{1 + N_m} \sqrt{\frac{1 - N/N_m}{1 + N}}, \tag{3.18}$$

and $N \equiv n - 1$ is the relative density fluctuation, $D \equiv -\sqrt{(6 + 2N_m)/N_m}$, and the boundary condition $N = N_m$ at $\eta = 0$ has been used without loss of generality. This solution describes a dip density soliton with an amplitude N_m, characteristic width $\Delta\eta \sim$ a few of $k_x D$, and a symmetrical center at $\eta = 0$.

The perturbed electric and magnetic fields (E_x, E_z, and B_y) of the corresponding inertial-regime SKAW can be given by Wu et al. (1995):

$$E_z = \pm \frac{D}{3} \left(\frac{-N_m}{1 + N_m}\right)^2 \left(1 - \tanh^2 Y\right) \tanh Y \cot\theta, \tag{3.19}$$

$$E_x = \pm D \frac{-N_m}{(1 + N_m)^2} \left(1 + \frac{N_m}{3} \tanh^2 Y\right) \tanh Y, \tag{3.20}$$

$$B_y = \pm D \frac{-N_m}{1 + N_m} \sqrt{\frac{1 + N_m/3}{1 + N_m}} \tanh Y, \tag{3.21}$$

where θ is the propagation angle of the SKAW, that is, $\cot\theta = k_z/k_x$, and the electric and magnetic fields are normalized by $\sqrt{Q} v_A B_0$ and $\sqrt{Q} B_0$, respectively.

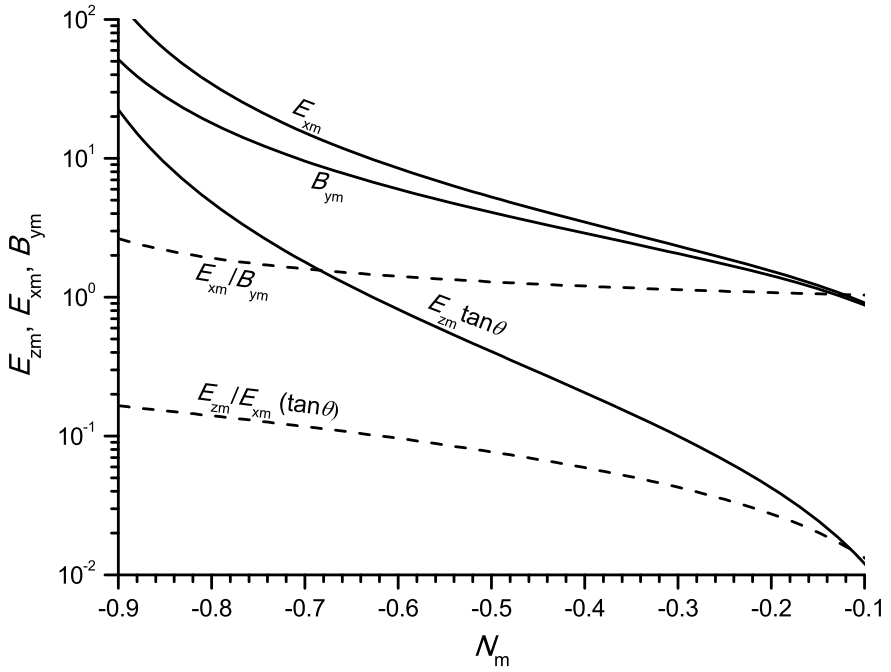

Fig. 3.8 Amplitudes of perturbed electric and magnetic fields of SKAWs versus the density amplitude N_m (from Wu 2012)

Figure 3.8 plots the amplitudes of perturbed electric and magnetic fields of SKAW versus the relative density amplitude N_m, where solid lines are the amplitudes of the parallel and transverse electric fields E_{zm} (amplified by $\tan\theta$) and E_{xm} (in units of $\sqrt{Q}v_A B_0$) and the transverse magnetic field B_{ym} (in units of $\sqrt{Q}B_0$), and two dashed lines are the ratios of the transverse electric to magnetic fields E_{xm}/B_{ym} (in units of the Alfvén velocity v_A) and the parallel to transverse electric fields E_{zm}/E_{xm} (amplified by $\tan\theta$). From Fig. 3.8, in a wide range of the density amplitude (i.e., $0.1 < |N_m| < 0.9$) the transverse electric and magnetic fields of SKAWs have amplitudes, E_{xm} and B_{ym}, several times of $\sqrt{Q}v_A B_0$ and $\sqrt{Q}B_0$, respectively. However, the parallel electric field E_{zm} has a wider varying range from lower than 0.1 when $|N_m| \sim 0.1$ to higher than 10 of $\sqrt{Q}v_A B_0$ when $|N_m| \sim 0.9$. Also Fig. 3.8 shows that the transverse electric to magnetic field ratio, E_{xm}/B_{ym}, is slightly higher than the Alfvén velocity v_A (i.e., ~1–2 v_A for $|N_m|$ between 0.1 and 0.9), as shown by the in situ observations by the FAST satellite (see Fig. 3.7). In addition, the parallel to transverse electric field ratio, E_{zm}/E_{xm} by a factor of $\tan\theta$, is about ~0.1.

In the auroral plasma environment explored by the Freja and FAST satellites at the altitude $\sim 0.3R_E$, one has $B_0 \simeq 0.2$ G, $v_A \simeq 1 \times 10^7$ m/s, and $Q \simeq 3.4 \times 10^{-5}$ (the ion component is dominated by O^+). This leads to $\sqrt{Q}v_A B_0 \sim 1$ V/m and $\sqrt{Q}B_0 \sim 100$ nT. The comparison with the observations by the Freja and FAST

satellites shows that the exactly analytical solution of the one-dimensional inertial-regime SKAWs can qualitatively describe the main physical properties of the strong electromagnetic spikes accompanied by strong density fluctuations presented in these satellites in situ observations. However, as shown both by the satellite observations in the space plasma (Chmyrev et al. 1988; Volwerk et al. 1996; Wu et al. 1996a, 1997) and the experimental measurements in the LAPD (Burke et al. 2000a, b), these strong electromagnetic spikes, in fact, are two-dimensional vortex structures, which are accompanied by dipole density solitons (Wu et al. 1996a, 1997).

The satellite observations in the space plasma (Chmyrev et al. 1988; Volwerk et al. 1996) and the experimental measurements in the LAPD (Burke et al. 2000a, b) both show that these two-dimensional vortex structures often present in an inhomogeneous ambient plasma. Taking account of the weak inhomogeneity of the ambient plasma in density, Wu et al. (1996a, 1997) proposed a two-dimensional SKAW model that has a dipole-vortex electromagnetic structure and is accompanied by a dipole density soliton. Its electromagnetic structures can be described by two scalar potentials, ϕ and ψ, as following:

$$\begin{aligned}\phi(r,\theta) &= ur_0B_0\left[1+a(l_0,l_1)\right]\frac{K_1(l_0R)}{K_1(l_0)}\cos\theta,\ \text{for } R>1\\ \phi(r,\theta) &= ur_0B_0\left[R+a(l_0,l_1)\frac{J_1(l_1R)}{J_1(l_1)}\right]\cos\theta,\ \text{for } R<1,\end{aligned}\tag{3.22}$$

and

$$\begin{aligned}\psi(r,\theta) &= r_0B_0\gamma\left[1+a(l_0,l_1)\frac{u}{\gamma v_A}\right]\frac{K_1(l_0R)}{K_1(l_0)}\cos\theta,\ \text{for } R>1\\ \psi(r,\theta) &= r_0B_0\gamma\left[R+a(l_0,l_1)\frac{u}{\gamma v_A}\frac{J_1(l_1R)}{J_1(l_1)}\right]\cos\theta,\ \text{for } R<1,\end{aligned}\tag{3.23}$$

where the polar ordinates $(r,\ \theta)$ is determined by

$$x = r\cos\theta \text{ and } \eta = r\sin\theta,\tag{3.24}$$

$\eta \equiv k_y y + k_z z - \omega t$ is the traveling-wave frame, the x-axis directs the inhomogeneity of the ambient plasma density, $R \equiv r/r_0$, r_0 is the characteristic radius for the localized two-dimensional vortex structure, $u = \omega/k_y$ is the characteristic perpendicular propagation velocity, and $\gamma = k_z/k_y$ represents the propagating direction. In addition, in above the expressions (x, y), z, t have been normalized by ρ_s, λ_i, and ω_{ci}^{-1}, respectively, the parameter $a(l_0, l_1)$ is determined by

$$a(l_0,l_1) = -\frac{l_0^2}{\left(2+l_0^2+l_1^2\right)J_1(l_1)},\tag{3.25}$$

l_0 and l_1 are related by:

$$\frac{K_0(l_0)}{l_0 K_1(l_0)} + \frac{2}{l_0^2} = \frac{l_1}{2+l_1^2}\frac{J_0(l_1)}{J_1(l_1)} - \frac{2}{2+l_1^2}, \tag{3.26}$$

and $J_{1(0)}$ and $K_{1(0)}$ are the first (zero) order Bessel function and the first (zero) order modified second kind Bessel function, respectively. Finally, the electric and magnetic fields of the vortex structure can be given by the two scalar potentials as follows:

$$\begin{aligned} &\mathbf{E}_\perp = -\nabla_\perp \phi, \quad E_\parallel = \hat{\mathbf{b}} \cdot \mathbf{E} = -\frac{d\phi}{dz} - \frac{\partial \psi}{\partial t}, \\ &\mathbf{B}_\perp = \nabla \times \left(\psi \hat{\mathbf{z}}\right) = \nabla_\perp \psi \times \hat{\mathbf{z}}. \end{aligned} \tag{3.27}$$

In particular, the relative perturbed density $N \equiv n - 1$ can be obtained as follows (Wu et al. 1996a, 1997):

$$\begin{aligned} N &= \left[R - (1 + a(l_0, l_1))\frac{K_1(l_0 R)}{K_1(l_0)}\right]\frac{r_0 \cos\theta}{L}, \quad \text{for } R > 1 \\ N &= -a(l_0, l_1)\frac{J_1(l_1 R)}{J_1(l_1)}\frac{r_0 \cos\theta}{L}, \qquad\qquad \text{for } R < 1, \end{aligned} \tag{3.28}$$

where, assuming the weak inhomogeneity of the ambient plasma with the characteristic scale $L \gg r_0$ in the x direction, the boundary condition $N = x/L$ for $r \to \infty$ has been used, the density continuity condition at $r = r_0$ leads to the perpendicular propagation velocity u as follows:

$$u = \frac{2}{l_1^2}\frac{r_0^2}{\rho_s L} v_s = \frac{2}{l_1^2}\frac{\omega_{ci} r_0^2}{L}. \tag{3.29}$$

Figure 3.9 shows the local density distribution inside the dipole vortex structure with the typical parameters $l_1 = 4$, $l_0 = 1.6$, $a(l_0, l_1) = 1.9$, and the density amplitude $N_m \sim 50\%$, where (a) is the whole picture of its two dimensional structure, (b) its contours, and (c) observed three kinds of density solitons when the satellite crosses the dipole vortex at the three different positions and directions denoted by S_1, S_2, and S_3 in (b), which correspond to the dip (S_1), hump (S_2), and dipole (S_3) density solitons, respectively. For the ambient plasma of the Freja satellite environment, the typical parameters may be taken as $T_e \sim 10$ eV, $B_0 \sim 0.3$ G, $L \sim 10$ km, $n_0 \sim 10^3$ cm^{-3}, and the average mass number of ions (mainly by the oxygen ions and the hydrogen ions) $\bar{\mu} \sim 7$, hence $v_s \sim 10$ km/s, $\rho_s \sim 30$ m. The typical scale of SKAWs may be taken as $r_0 \sim 10\rho_s \sim 300$ m. From Fig. 3.7, it can be found that these density solitons have a spatial scale length of $\sim$1–2r_0, which is comparable with observations of the Freja satellite.

The perturbed electric and magnetic fields inside the dipole vortex structure can be obtained by Eq. (3.27) as follows:

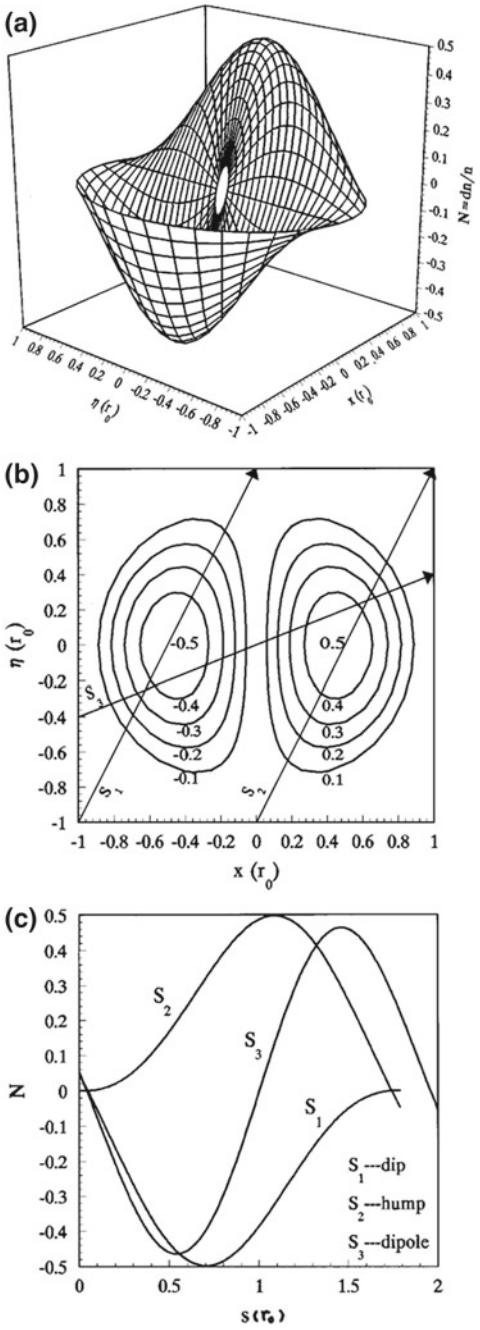

Fig. 3.9 **a** The two-dimensional density distribution in a dipole vortex structure; **b** The contours of the density distribution and three possible cases of the satellite crossing the dipole vortex structure at loci S_1, S_2 and S_3; **c** The dip, hump, and dipole density solitons observed by the satellite, respectively, at loci S_1, S_2, and S_3 (reprinted from Wu et al., Phys. Plasmas, 4, 611–617, 1997, with the permission of AIP Publishing)

$$
\begin{aligned}
E_y &= -uB_0 \frac{a(l_0, l_1)}{2} \left(\frac{l_1 J_0(l_1 R)}{J_1(l_1)} - \frac{J_1(l_1 R)}{R J_1(l_1)} \right) \sin 2\theta, \\
E_x &= -uB_0 \left[1 + a(l_0, l_1) \left(\frac{l_1 J_0(l_1 R)}{J_1(l_1)} \cos^2 \theta - \frac{J_1(l_1 R)}{R J_1(l_1)} \cos 2\theta \right) \right], \\
E_z &= \left(\gamma - \frac{u}{v_A} \right) E_y, \\
B_x &= -\frac{E_y}{v_A}, \quad B_y = \frac{E'_x}{v_A} - \gamma B_0.
\end{aligned} \tag{3.30}
$$

In particular, the peak values of the perturbed electric fields can be obtained from Eq. (3.30) as follows:

$$
E'_{xm} \equiv E_{xm} + uB_0 = 2E_{ym} = 2uB_0 \frac{a(l_0, l_1) l_1}{4J_1(l_1)} = 2uB_0 \frac{l_1 N_m}{4J_{1m}} \frac{L}{r_0}. \tag{3.31}
$$

From Eq. (3.30), one has the field-aligned component of perturbed electric fields, E_z, much less than their cross-field components, E_x and E_y, that is, $|E_\parallel / E_\perp| \ll 1$, which is consistent with that in one-dimensional SKAWs. Unlike to those of one-dimensional SKAWs, however, the perturbed electric fields of two-dimensional SKAWs are no longer plane polarization. Figure 3.10 shows the "rotation" curves of the perturbed electric fields in the plane perpendicular to the magnetic field. It can be found that the "rotation" direction of perturbed electric fields of dip density solitons is opposite to that of hump density solitons, while perturbed electric fields of dipole density solitons twice undergo opposite "rotation."

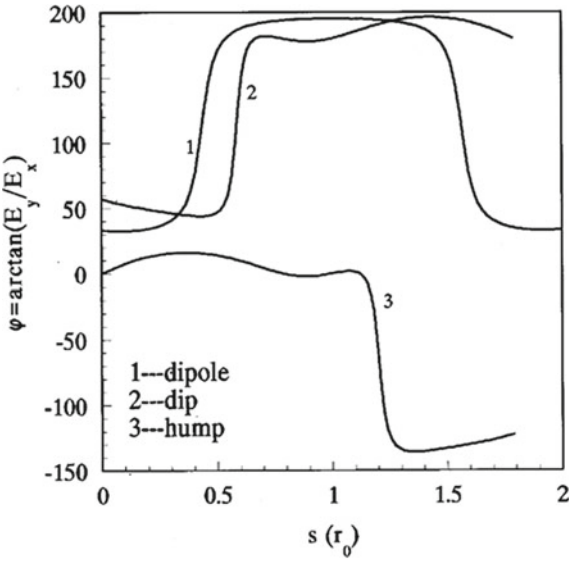

Fig. 3.10 The "rotation" curves of perturbed electric fields associated with dip, hump, and dipole density solitons (reprinted from Wu et al., Phys. Plasmas, 4, 611–617, 1997, with the permission of AIP Publishing)

In comparison to one-dimensional SKAWs, the most important unique feature of two-dimensional SKAWs is that they have vortex structures. In particular, the two-dimensional SKAWs with dipole vortex structures can permit the presence of not only single dip or hump density solitons but also dipole density solitons, while the latter can not present in one-dimensional SKAWs. Second, the polarization of their perturbed electromagnetic fields is no longer plane polarization, which is obviously distinct from that of one-dimensional SKAWs, and has a "rotation" feature, as shown by analyses of the Freja observations (Volwerk et al. 1996). These results indicate that the model of two-dimensional SKAWs with dipole vortex structures can provide us more self-consistent physical explanation for SKAW phenomena in space plasmas, although the one-dimensional SKAW model can well explain their main properties observed by satellites in space plasmas.

3.5 Auroral Electron Acceleration by SKAWs

In a collisionless plasma environment such as the auroral plasma, especially in the auroral acceleration region, in general, the very large parallel conductivity can immediately short-circuit any parallel electric fields. Therefore, one of key difficulties in understanding the physics of the auroral electron acceleration is how to produce and maintain a large parallel electric field that can accelerate field-aligned electrons to keV-order energies (Fälthammar 2004). Now that a field-aligned electric field can develop within KAWs observed commonly in the auroral plasma, they have been proposed by many authors as one of possible acceleration mechanisms for producing auroral electrons (Chmyrev et al. 1988; Goertz 1981, 1984; Goertz and Boswell 1979; Hasegawa 1976; Hasegawa and Mima 1978; Hui and Seyler 1992; Kivelson and Southwood 1986; Kletzing 1994; Lee et al. 1994; Lysak and Carlson 1981; Lysak and Dum 1983; Thompson and Lysak 1996). However, the detailed physical mechanism has been an open problem. Wu (2003a, b) and Wu and Chao (2003, 2004) proposed that SKAWs can play an important role in the auroral electron acceleration, in which effective parallel electric fields can be maintained by the inertial motion of electrons along the magnetic field.

In fact, some further data analyses have clearly revealed that SKAWs observed in the auroral plasma are often associated with enhanced broadband electrostatic fluctuations, which can be identified well as ion-acoustic turbulence. The accompanied ion-acoustic turbulence will possibly cause the dissipation of the SKAWs and lead to their dynamical evolution and deformation. For example, based on the analysis of a large number of events associated with SKAWs observed by Freja, Wahlund et al. (1994a) found that these associated SKAWs could be classified into three different observational phases and proposed that they are possibly responsible for three different stages in the dynamical evolution of SKAWs. The first stage is the "ordinary" SKAW, the second stage is the SKAW accompanied with enhanced broadband electrostatic fluctuations in the ion-acoustic wave mode, and in the third stage, the SKAW has been transformed into an electrostatic-like structure.

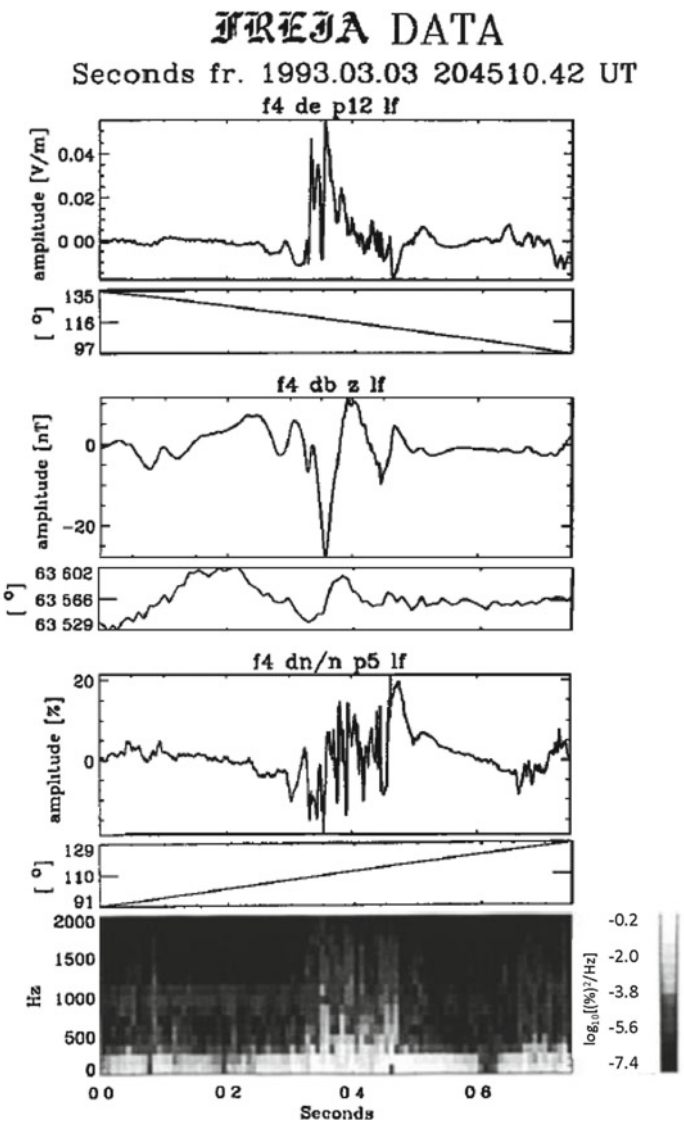

Fig. 3.11 An example of a SKAW filled by enhanced broadband electrostatic turbulence in the ion-acoustic mode (from Wahlund et al. 1994a)

Figure 3.11 shows a clear example of the second stage SKAW, in which a well defined SKAW with $\delta E \sim 60$ mV/m, $\delta B \sim 15$ nT, and $dn/n \sim 30\%$ is detected between 0.3 and 0.5 s, but in contrast to the first stage ordinary SKAW, it also contains enhanced broadband electrostatic and density fluctuations, which can be identified well as enhanced ion-acoustic turbulence (Wahlund et al. 1994a, b). Based on these

observations, Wu (2003a, b) proposed that the enhanced ion-acoustic turbulence of accompanying the second stage SKAW can be excited by the electrostatic instability of the electrons trapped inside the SKAW, which are accelerated by the parallel oscillational electric field of the SKAW to an v_A-order field-aligned velocity, especially in the inertial-regime SKAW case, these trapped electrons can have a field-aligned velocity larger than the thermal velocity of the ambient electrons. Then the enhanced ion-acoustic turbulence causes effective dissipation of the SKAW through the wave-particle interaction and leads to the SKAW further evolving into an electrostatic-like structure, that is, the third stage SKAW.

In order to take account of the effect of the enhanced ion-acoustic turbulence on the dynamical evolution of SKAWs, Wu (2003a, b) invoked an anomalous collisional damping term of the electrons in their field-aligned momentum equation, which is caused by the wave-particle interaction due to the enhanced ion-acoustic turbulence and may be described by the following "effective collisional frequency", ν_e, Hasegawa (1975):

$$\nu_e = \frac{W_{ia}}{n_0 T_e}\omega_{pe}, \tag{3.32}$$

where W_{ia} is the energy density of the enhanced ion-acoustic turbulence. Including this "anomalous dissipation" effect due to the enhanced ion-acoustic turbulence, the Sagdeev equation of governing the SKAW dynamics can be written as follows (Wu 2003a, b):

$$\frac{d}{d(-\eta)}\left[\frac{1}{2}\left(\frac{d}{d\eta}\frac{2}{n^2}\right)^2 + \frac{K(n)}{n^6}\right] = -\gamma\left(\frac{d}{d\eta}\frac{2}{n^2}\right)^2, \tag{3.33}$$

where the Sagdeev potential for the inertial-regime SKAWs

$$K(n; M_z, k_x) = -\frac{n^3(n-1)^2}{3M_z^2 k_x^2}\left(\frac{n}{n_m} - 1\right) \tag{3.34}$$

with the density amplitude

$$n_m = \frac{2}{3M_z^2 - 1} < 1 \tag{3.35}$$

and the "damping coefficient" of describing the anomalous dissipation effect

$$\gamma \equiv \frac{\sqrt{Q}}{M_z k_z}\frac{\nu_e}{\omega_{ci}}. \tag{3.36}$$

It is clear that when neglecting the anomalous dissipation effect ($\gamma = 0$) the Sagdeev equation for the inertial-regime SKAWs can be recovered from the integral of Eq. (3.33).

In analogy to the Sagdeev equation (3.8), Eq. (3.33) also describes the motion of a "classical particle" in the "potential well" $K(n)/n^6$, with "time" $t = -\eta$, "space"

$x = 2/n^2$, hence "velocity" $dx/dt = -d\left(2/n^2\right)/d\eta$. The "classical particle" can conserve its energy when $\gamma = 0$. Only if $\gamma > 0$ (independent of specific values of γ), the "damping" $-\gamma\left(dx/dt\right)^2 = -\gamma\left(d\left(2/n^2\right)/d\eta\right)^2$ will make the "particle" lose gradually its "energy" and ultimately stay at the bottom of the "potential well" $K(n)/n^6$ when $t = -\eta \to +\infty$. The "position" $n = n_d$ of the bottom can be obtained by the condition that the potential energy $K(n)/n^6$ reaches its minimum as follows:

$$n_d = \frac{3n_m}{2 + n_m} = \frac{1}{M_z^2} > n_m. \tag{3.37}$$

This result indicates that the density structure of the dissipated SKAW (DSKAW), described by Eq. (3.33) has the asymptotic values $n \to n_d$ and $n \to 1$ when $\eta \to -\infty$ and $\eta \to \infty$, respectively. In other words, the density profile of DSKAWs has a shock-like structure with a density jump

$$\Delta n \equiv 1 - n_d = 1 - \frac{1}{M_z^2} = \frac{2|N_m|}{3 + N_m} < |N_m|, \tag{3.38}$$

where $N_m \equiv n_m - 1$.

Figure 3.12 illustrates density behaviors of DSKAWs with the damping coefficient $\gamma = 1.00, 0.50, 0.10, 0.05, 0.02$, and 0.01 from the top down, where the parameters $k_x/k = \sin 89^\circ$ for the quasi-perpendicular propagating angle $\theta = 89^\circ$, and $M_z = 1.29$ for the density amplitude $n_m \simeq 0.5$ have been used. For the sake of comparison, dashed lines in Fig. 3.12 show the density soliton solutions of SKAWs with the same parameters except for $\gamma = 0$.

From Fig. 3.12, it can be found that the density of DSKAWs behaves itself like an ordinary "shock" with a density jump $\Delta n \simeq 0.4$ for a strong dissipation case of $\gamma \sim 1$. For a weakly dissipative regime of $\gamma \ll 1$, however, the density waveform appears to be a train of oscillatory waves with amplitude decreasing in the downstream of $\eta < 0$ and converges upon an ultimate downstream density $n_d \simeq 0.6$ when $\eta \to -\infty$ and, as a result, a local shock-like structure with the same density jump ($\Delta n = 1 - n_d \simeq 0.4$) is formed. It is worth noticing that the ultimate density n_d and hence the density jump Δn are independent of the damping coefficient γ. In fact, the magnitude of γ affects only the oscillating strength and the converging speed in the manner that the lower γ leads to the stronger oscillation and the slower convergence.

At the ultimate downstream state of DSKAWs, the field-aligned "escape" velocity of the electrons trapped inside DSKAWs is given by Wu (2003a, b)

$$v_{ed} \equiv v_{ez}|_{n=n_d} = \left(1 - M_z^2\right) M_z v_A = -\frac{\Delta n}{(1 - \Delta n)^{3/2}} v_A, \tag{3.39}$$

which implies the electrons accelerated inside the DSKAW can escape from the downstream at the velocity v_{ed}, in contrast to the case of SKAWs, where the accelerated electrons are, at all, trapped inside the SKAW. These escaping electrons are

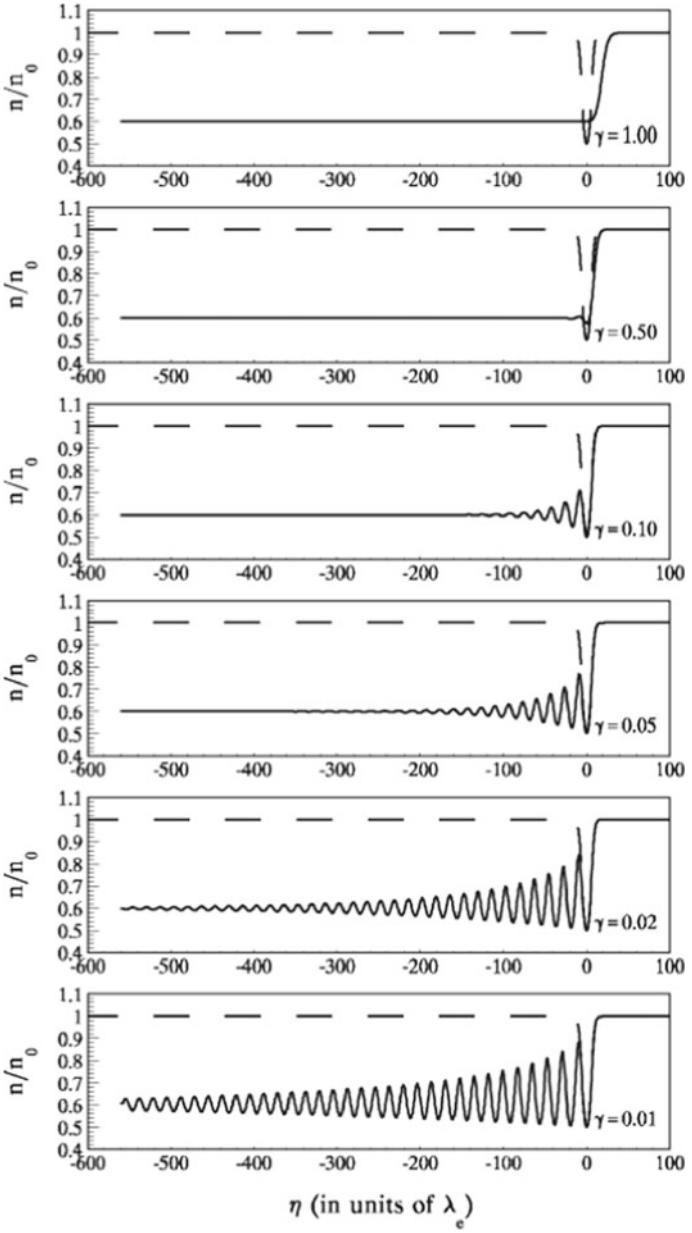

Fig. 3.12 Density distributions of DSKAWs (normalized to n_0) with the parameters $\theta = 89°$, $M_z = 1.29$, and $\gamma = 1, 0.5, 0.1, 0.05, 0.02$, and 0.01, from the top down. Dashed lines represent the density of SKAWs with the same parameters as DSKAWs except for $\gamma = 0$ (reprinted from Wu, Phys. Plasmas, 10, 1364–1370, 2003b, with the permission of AIP Publishing)

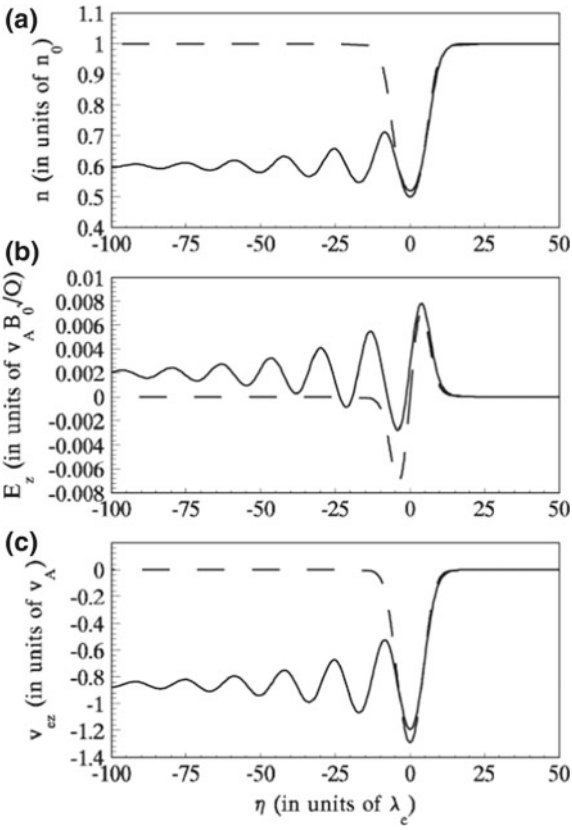

Fig. 3.13 Sketch of the shock-like structure of the DSKAW for the parameters $\theta = 89°$, $M_z = 1.29$, and $\gamma = 0.1$: **a** the density n (normalized to n_0); **b** the field-aligned electric field E_z (normalized to $\sqrt{Q}v_A B_0$); and **c** the electron velocity v_{ez} (normalized to v_A). Dashed lines represent the corresponding solutions of the SKAW with the same parameters except for $\gamma = 0$ (reprinted the figure with permission from Wu, Phys. Rev. E 67, 027402, 2003a, copyright 2003 by the American Physical Society)

accelerated by the field-aligned electric field E_z of the DSKAW, which nonsymmetrically distributes about the center $\eta = 0$.

Figure 3.13 shows the distributions of the density n (a), the field-aligned electric field E_z (b), and the electron velocity v_{ez} (c) in DSKAW with parameters $\theta = 89°$, $M_z = 1.29$, and $\gamma = 0.1$. For the sake of comparison, the solutions of the corresponding SKAW with the same parameters are presented by the dashed lines in Fig. 3.13. From Fig. 3.13b, it can be found that the electric field E_z varies no longer symmetrically about the center $\eta = 0$, and has a nonsymmetrical structure. In particular, the electric field E_z, although oscillating, has a preferential direction of $E_z > 0$ at the downstream, and leads to the electrons to be accelerated towards the downstream, then to get over the collisional resistance at the downstream, and ultimately to escape from the downstream at the velocity v_{ed}, as shown in Fig. 3.13c.

From Eq. (3.39), the escaping velocity of the electrons accelerated by DSKAWs, and hence their escaping energies increase with the increase of the density jump Δn of the DSKAWs and have typically the order of v_A, as expected. In fact, the escaping

velocity v_{ed} has magnitudes of ~0.1–10 v_A for a wider Δn through 0.1–0.8. From Eq. (3.39), the energy of the escaping electrons can be given by

$$\varepsilon_{ed} \equiv \frac{1}{2} m_e v_{ed}^2 = \left(M_z^2 - 1\right)^2 M_z^2 \varepsilon_{eA} = \frac{\Delta n^2}{(1-\Delta n)^3} \varepsilon_{eA}, \tag{3.40}$$

where $\varepsilon_{eA} \equiv m_e v_A^2/2$ is the energy of the electron moving at the Alfvén velocity, called the "electron Alfvén energy", which represents the characteristic energy of the escaping electrons accelerated by a typical DSKAW and is determined by the local Alfvén velocity of the ambient plasma. This indicates that the energy of the electrons accelerated by DSKAWs evidently depends on the local Alfvén velocity (i.e., directly proportional to the electron Alfvén energy ε_{eA}) and ranges ~0.1–10ε_{eA} for the DSKAWs with density jumps $\Delta n \sim 22$–65%.

Figure 3.14a presents the variation of the electron Alfvén energy ε_{eA} (in keV), based on the altitude model of the ambient auroral plasma presented in Fig. 3.4. From Fig. 3.14a it can be found that the electron Alfvén energy ε_{eA} has higher values ~1–5 keV in the observed acceleration region of $h \sim 0.5$–$2R_E$, which is the typical characteristic energies of the auroral energetic electrons as shown by observed (see Fig. 3.3), and reaches the maximal value ≃5.3 keV at $h \simeq 0.82R_E$. It is evident that the higher local Alfvén velocity, and hence the higher electron Alfvén energy, leads to the higher escaping energy of the accelerated electrons in the DSKAW acceleration mechanism. However, in the observations of SKAWs the strong DSKAWs with $\Delta n > 50\%$ usually are rather rare, which leads to the escaping energy of the accelerated $\varepsilon_{ed} \simeq 2\varepsilon_{eA}$, that is, $\varepsilon_{ed} \sim 10.6$ keV for the maximal $\varepsilon_{eA} \simeq 5.3$ keV in the auroral acceleration region. This implies that the highest energy of the auroral energetic electrons accelerated by DSKAWs is ~10.6 keV, and above this energy the auroral energetic electron flux will precipitously decrease because of the absence of extremely strong DSKAWs with density jump $\Delta n > 50\%$ (Bryant 1981). The result presented in Fig. 3.14a indicates that, in the observed auroral acceleration region, the observed DSKAWs accompanied by moderately strong density jumps can effectively accelerate the electrons to the typical keV-order energies of the auroral energetic electrons.

On the other hand, the enhanced electrostatic ion-acoustic turbulence plays an important role in the dynamical evolution of SKAWs towards DSKAWs (Wahlund et al. 1994a). In the case of inertial-regime SKAWs, the enhanced electrostatic turbulence can be effectively excited by the electrostatic instability of the electrons that are trapped in the potential well of the SKAWs and have the typical v_A-order field-aligned velocity evidently higher than the local thermal speed of the ambient plasma (Wu 2003a, b; Wu and Chao 2003, 2004). In particular, the lower parameter α_e (hence the higher velocity ratio v_A/v_{T_e}) leads to the more efficient excitation of the enhanced electrostatic turbulence and the more effectively dynamical evolution of SKAWs towards DSKAWs. Figure 3.4e clearly shows that there is the lower parameter $\alpha_e \ll 1$ in the observed auroral acceleration region, implying that the plasma environment in the observed acceleration region is more favorable of the formation

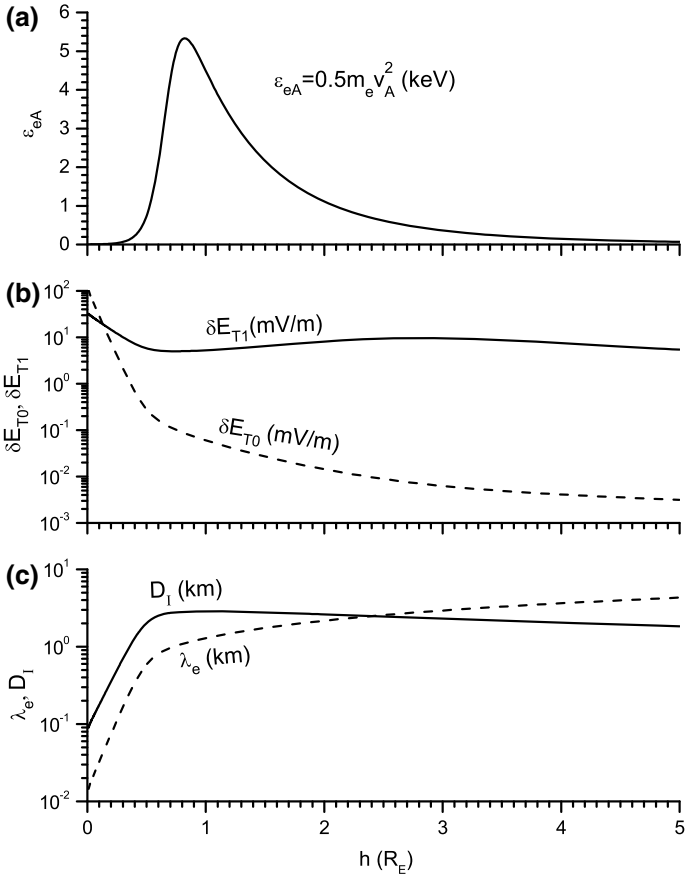

Fig. 3.14 The altitude distribution of the characteristic parameters of the DSKAW acceleration mechanism: the electron Alfvén energy ε_{eA} in keV (**a**), the electrostatic ion-acoustic turbulence δE_{T1} (dashed line) and δE_{T0} (dashed line) in mV/m (**b**), and field-aligned projection of the characteristic width of DSKAWs on the ionosphere D_I (solid line) and the electron inertial length λ_e (dashed line) (**c**)

of DSKAWs. In order to produce the sufficient "anomalous dissipation" to cause SKAWs efficiently evolving into DSKAWs, the strength of the enhanced electrostatic ion-acoustic turbulence, δE_T, is required to be considerably higher than its thermal noise level, δE_{T0}, on which the effective collision frequency in Eq. (3.32) is equal to the classic collision frequency, that is, $\nu_e = \nu_c$ (Hasegawa 1975):

$$\delta E_{T0} \simeq 0.94 \times 10^{-2} T_e^{-1/4} n_0^{3/4} \text{ mV/m}, \tag{3.41}$$

where T_e is in units eV and n_0 is in cm^{-3}. For example, in order to produce the damping coefficient of $\gamma = 0.1$, from Eq. (3.36) the requisite strength of the ion-acoustic turbulence δE_{T1} can be estimated by (Wu and Chao 2003, 2004)

$$\delta E_{T1} \simeq 5.53 n_0^{1/4} T_e^{1/2} B_0^{1/2} \text{ mV/m}. \tag{3.42}$$

Fig. 3.14b shows the variations of δE_{T0} (dashed line) and δE_{T1} (solid line) with the altitude h above the ionosphere. The former (i.e, the thermal noise level) corresponds to the turbulent wave strength that is able to produce an effective collision frequency $\nu_e = \nu_c$ (the classic collision frequency), and the latter does the strength that is able to produce an effective collisional frequency ν_e to result in a damping coefficient $\gamma = 0.1$. From Fig. 3.14b, one can find that $\delta E_{T1} < \delta E_{T0}$ in the ionosphere below $h \simeq 0.13 R_E$, implying that the classic collision dominates the collisional damping and can lead to the damping coefficient $\gamma > 0.1$ in the denser ionosphere below $h \simeq 1.3 R_E$. While in the tenuous magnetosphere above $h \simeq 0.13 R_E$ the dissipation damping is dominated by the effective collision due to the ion-acoustic turbulence. In particular, for the auroral acceleration region of $h \sim 0.5$–$2 R_E$, Fig. 3.14b shows that the damping coefficient of $\gamma = 0.1$ needs the enhanced ion-acoustic turbulence strength $\delta E_{T1} \sim 5$–10 mV/m, which can be well satisfied by the observations of turbulent electric fields in the auroral plasma (Vaivads et al. 1998; Wahlund et al. 1994a, b, 1998).

The width of discrete auroral arcs produced by DSKAWs acceleration mechanism can be estimated from the field-aligned projection of the DSKAW width on the ionosphere because the accelerated auroral electrons precipitate field-aligned into the ionosphere. Both theory and observation (Chaston et al. 1999; Wu 2003b) show DSKAWs at the altitude h have a typical width $D \sim 2\pi\lambda_e(h)$, where $\lambda_e(h) = c/\omega_{pe}(h)$ is the local electron inertial length at the altitude h. The field-aligned projection of the DSKAW with the width $D(h)$ on the ionosphere $D_I(h)$ can be obtained by:

$$D_I(h) = \frac{2\pi\lambda_e(h)}{(1+h)^{3/2}}, \tag{3.43}$$

where the dipole field model of the Earth's magnetic field and the magnetic flux conservation along the polar field lines have been used. Figure 3.14c displays the altitude variations of the electron inertial length $\lambda_e(h)$ (dashed line) and the width of discrete auroral arcs produced by the DSKAW acceleration mechanism $D_I(h)$ (solid line). From Fig. 3.14c, it can be found that the auroral arcs produced by the electrons accelerated by DSKAWs from the auroral acceleration region of $h \sim 0.5$–$2 R_E$ can be expected to have a typical width $\sim$1–3 km in the ionosphere, which is comparable to the characteristic width of observed auroral arcs.

Based on the DSKAW acceleration mechanism of the auroral energetic electrons described above, it is possible that the main observed properties of the auroral energetic electrons, which had been mentioned in the beginning of this chapter, may be explained reasonably and uniformly as follows:

Field-aligned acceleration: In the DSKAW acceleration mechanism, it is the parallel electric field of the DSKAW that accelerates field-aligned the electrons to escape from the downstream of the shock-like structure of the DSKAW and to precipitate along the geomagnetic field on the ionosphere;

Characteristic energy: The characteristic energy of the electrons accelerated by the DSKAW acceleration mechanism is typically in the order of the electron Alfvén energy ε_{eA}, which reaches highest values in the auroral acceleration region of $h \sim 0.5$–$2R_E$ and has the typical energies of the auroral energetic electrons, that is, several keVs for the moderately strong DSKAWs observed most frequently in the auroral plasma;

High-energy cutoff: For the moderately strong DSKAWs with the density jump $\Delta n \sim 50\%$, the highest energy of the electrons accelerated by the DSKAW is ~ 10.6 keV in the auroral acceleration region, it is probably because of the absence of extremely strong DSKAWs with the density jump $\Delta n > 50\%$ that the auroral energetic electron flux precipitously decreases above 10 keV;

Acceleration region: The auroral acceleration region is located in the altitude of $h \sim 0.5$–$2R_E$ because both the Alfvén velocity and the ratio of the Alfvén velocity to the electron thermal speed reach highest there. The former leads to the DSKAW acceleration mechanism having a higher acceleration efficiency, that is, being able to accelerate the electrons to higher energies directly proportional to the square of the Alfvén velocity (i.e., the electron Alfvén energy), and the latter is more favorable of the excitation of the enhanced electrostatic ion-acoustic turbulence and hence of the formation of DSKAWs;

Discrete auroral arc: An individual DSKAW produces a discrete auroral arc, which width is the projection of the width of the corresponding DSKAW on the ionosphere along the geomagnetic field lines, that is, the observed width of typical auroral arcs $\sim$ a few km, as shown in Fig. 3.12c. A large number of observations show that special acceleration source regions of auroral energetic electrons usually come from some cavities with a lower density and hence with a higher Alfvén velocity in the center than that in the edge, and in result the auroral electrons accelerated by DSKAWs in the auroral arc center have higher energies than that in the auroral arc edge.

The auroral energetic acceleration mechanism is an essentially and crucially important problem, but not the whole problem in the auroral and substorm dynamics. Above the discussions show that the DSKAW acceleration mechanism can well explain reasonably and uniformly the main observed properties of the auroral energetic electrons. Based on this explanation we try to propose the following scenario for the auroral phenomena. Strong AWs or KAWs are produced by some generators, for instance, shear flows or pressure gradients in the CPS and PSBL (Borovsky 1993), which propagate into the auroral zone along the geomagnetic field lines and evolve into nonlinear structures, such as SKAWs. When entering into the auroral acceleration region of $h \sim 0.5$–$2R_E$ where is a lower density cavity, a higher ratio $v_A/v_{T_e} > 1$ leads to a higher field-aligned velocity of the electrons trapped inside the SKAWs, $v_{ez} \sim v_A > v_{T_e}$. These fast electrons can effectively excite electrostatic instabilities and lead to the formation of the enhanced electrostatic turbulence, such as the Langmuir wave or ion-acoustic wave turbulence. In consequence, the SKAWs dynamically evolve into the DSKAWs with shock-like structures due to the anomalous dissipation caused by the wave-particle interaction between the turbulent waves

and electrons. These DSKAWs are trapped in the auroral acceleration region due to the reflection by the ionosphere or by the Alfvén velocity gradient in the upper magnetosphere (Vogt and Haerendel 1998) and can effectively accelerate field-aligned electrons to escape from the downstream of the shock-like structures. Therefore, when propagating downwards or upwards these DSKAWs can accelerate electrons upwards or downwards and produce upgoing or downgoing energetic electron flows (i.e., field-aligned currents downwards or upwards, Boehm et al. 1995). The fast electrons travelling in the low-density cavity (i.e., the acceleration source region) produce AKR phenomena due to the electron-cyclotron maser instability, and when downgoing and impacting the dense ionosphere or the upper atmosphere they lead to visible auroras.

References

Akasofu, S.-I. (1981). Energy coupling between the solar wind and the magnetosphere. *Space Science Reviews*, *28*, 121–190.

Alfvén, H. (1957). On the theory of comet tails. *Tellus*, *1*, 92–96.

Banks, P. M., & Holzer, T. E. (1969). High-latitude plasma transport: The polar wind. *Journal of Geophysical Research*, *74*, 6317–6332.

Bellan, P. M., & Stasiewicz, K. (1998). Fine-scale cavitation of ionospheric plasma caused by inertial Alfvén wave ponderomoive force. *Physical Review Letters*, *80*, 3523–3526.

Biermann, L. (1948). Über die Ursache der chromosphärischen Turblenz und des UV-Exzesses der Sonnenstrahlung. *Zeitschrift fur Astrophysik*, *25*, 161–169.

Biermann, L. (1951). Kometenschweife und solare Korpuskular Strahlung. *Zeitschrift fur Astrophysik*, *29*, 274–286.

Biermann, L. (1957). Solar corpuscular radiation and the interplanetary gas. *Observatory*, *77*, 109–110.

Bingham, R., Bryant, D. A., & Hall, D. S. (1984). A wave model for the aurora. *Geophysical Research Letters*, *11*, 327–330.

Birkeland, K. R. (1908). *The norwegian aurora polaris expedition 1902–1903: On the cause of magnetic storms and the origin of terrestrial magnetism*. London: Longmans Green & Co.

Boehm, M. H., Clemmons, J., Wahlund, J. E., et al. (1995). Observations of an upward-directed electron beam with the perpendicular temperature of the cold ionosphere. *Geophysical Research Letters*, *22*, 2103–2106.

Bonetti, A., Bridge, H. S., Lazarus, A. J., Lyon, E. F., Rossi, B., & Scherb, F. (1963). Explorer 10 plasma measurements. *Journal of Geophysical Research*, *68*, 4017–4063.

Borovsky, J. E. (1993). Auroral arc thicknesses as predicted by various theories. *Journal of Geophysical Research: Space Physics*, *98*, 6101–6138.

Boström, R., Gustafsson, G., Holback, B., et al. (1988). Characteristics of solitary waves and weak double layers in the magnetospheric plasma. *Physical Review Letters*, *61*, 82–85.

Bridge, H. S., Dilworth, C., Lazarus, A. J., Lyon, E. F., Rossi, B. & Scherb, F. (1962). Direct observations of the interplanetary plasma. *Journal of the Physical Society of Japan*, *17*(Suppl. A-II), 553.

Bryant, D. A. (1981). Rocket studies of particle structure associated with auroral arcs. In Akasofu & Kan (Eds.), *AGU geophysical monographs 25: Physics of auroral arc formation* (p. 103).

Bryant, D. A. (1990). Two theories of auroral electron acceleration. In Buti (Ed.), *Solar and planetary plasma physics* (pp. 58–91). London: World Scientific.

Burke, A. T., Maggs, J. E., & Morales, G. J. (2000a). Spontaneous fluctuations of a temperature filament in a magnetized plasma. *Physical Review Letters*, *84*, 1451–1454.
Burke, A. T., Maggs, J. E., & Morales, G. J. (2000b). Experimental study of fluctuations excited by a narrow temperature filament in a magnetized plasma. *Physics of Plasmas*, *7*, 1397–1407.
Carlson, C. W., Pfaff, R. E., & Watzin, J. G. (1998). The fast auroral SnapshoT (FAST) mission. *Geophysical Research Letters*, *25*, 2013–2106.
Chapman, S. (1931a). The absorption and dissociative or ionizing effect of monochromatic radiation in an atmosphere on a rotating earth. *Proceedings of the Physical Society*, *43*, 26–45.
Chapman, S. (1931b). The absorption and dissociative or ionizing effect of monochromatic radiation in an atmosphere on a rotating earth part II. Grazing incidence. *Proceedings of the Physical Society*, *43*, 483–501.
Chapman, S., & Ferraro, V. C. A. (1930). A new theory of magnetic storms. *Nature*, *126*, 129–130.
Chapman, S., & Ferraro, V. C. A. (1931). A new theory of magnetic storms. *Terrestrial Magnetism and Atmospheric Electricity*, *36*, 77.
Chaston, C. C., Carlson, C. W., Peria, W. J., et al. (1999). FAST observations of inertial Alfvén waves in the dayside aurora. *Geophysical Research Letters*, *26*, 647–650.
Chian, C. L., & Kamide, Y. (2007). An overview of the solar-terrestrial environment. In Y. Kamide & A. Chian (Eds.), *Handbook of the solar-terrestrial environment* (pp. 1–23). Berlin: Springer.
Chmyrev, V. M., Bilichenko, S. V., Pokhotelov, O. A., et al. (1988). Alfvén vortices and related phenomena in the ionosphere and the magnetosphere. *Physica Scripta*, *38*, 841–854.
Fälthammar, C. G. (2004). Magnetic-field aligned electric fields in collisionless space plasmas-a brief review. *Geofisica Internacional*, *43*, 225–239.
Goertz, C. K. (1981). Discrete breakup arcs and kinetic Alfvén waves. In Akasofu & Kan (Eds.), *AGU geophysical monographs 25: Physics of auroral arc formation* (p. 451).
Goertz, C. K. (1984). Kinetic Alfvén waves on auroral field lines. *Planetary and Space Science*, *32*, 1387–1392.
Goertz, C. K., & Boswell, R. W. (1979). Magnetosphere-ionosphere coupling. *Journal of Geophysical Research*, *84*, 7239–7246.
Gold, T. (1959). Motions in the magnetosphere of the earth. *Journal of Geophysical Research*, *64*, 1219–1224.
Gurnett, D. A. (1974). The earth as a radio source-Terrestrial kilometric radiation. *Journal of Geophysical Research*, *79*, 4227–4238.
Hasegawa, A. (1975). *Plasma instabilities and nonlinear effects* (p. 93). New York: Springer.
Hasegawa, A. (1976). Particle acceleration by MHD surface wave and formation of aurora. *Journal of Geophysical Research*, *81*, 5083–5090.
Hasegawa, A., & Mima, K. (1976). Exact solitary Alfvén wave. *Physical Review Letters*, *37*, 690–693.
Hasegawa, A., & Mima, K. (1978). Anomolous transport produce by kinetic Alfvén wave turbulence. *Journal of Geophysical Research*, *83*, 1117–1123.
Heppner, J. P., Ness, N. F., Skillman T. L. & Scearce, C. S. (1962). Magnetic field measurements with the Explorer 10 satellite. *Journal of the Physical Society of Japan*, *17*(Suppl. A-II), 546.
Hoffman, R. A., & Evans, D. S. (1968). Field-aligned electron bursts at high latitude observed by OGO-4. *Journal of Geophysical Research*, *73*, 6201–6214.
Hoffmeister, C. (1943). Physikalische Untersuchungen an Kometen. I. Die Beziehungen des primären Schweifstrahls zum Radiusvektor. *Zeitschrift fur Astrophysik*, *22*, 265–285.
Huang, G. L., Wang, D. Y., Wu, D. J., et al. (1997). The eigenmode of solitary kinetic Alfvén waves by Freja satellite. *Journal of Geophysical Research*, *102*, 7217–7224.
Hui, C. H., & Seyler, C. E. (1992). Electron acceleration by Alfvén waves in the magnetosphere. *Journal of Geophysical Research*, *97*, 3953–3963.
Kalita, M. K., & Kalita, B. C. (1986). Finite-amplitude solitary Alfvén waves in a low-beta plasma. *Journal of Plasma Physics*, *35*, 267–272.
Kivelson, M. G., & Southwood, D. J. (1986). Coupling of global magnetospheric MHD eigenmodes to field line resonance. *Journal of Geophysical Research*, *91*, 4345–4351.

Kletzing, C. A. (1994). Electron acceleration by kinetic Alfvén waves. *Journal of Geophysical Research*, *99*, 11095–11103.
Kletzing, C. A., & Torbert, R. B. (1994). Electron time dispersion. *Journal of Geophysical Research*, *99*, 2159–2172.
Kletzing, C. A., Mozer, F. S., & Torbert, R. B. (1998). Electron temperature and density at high latitude. *Journal of Geophysical Research*, *103*, 14837–14845.
Kletzing, C. A., Scudder, J. D., Dors, E. E., & Curto, C. (2003). Auroral source region: Plasma properties of the high-latitude plasma sheet. *Journal of Geophysical Research*, *108*, 1360–1375.
Lee, L. C., & Wu, C. S. (1980). Amplification of radiation near cyclotron frequency due to electron population inversion. *The Physics of Fluids*, *23*, 1348.
Lee, L. C., Johnson, J. R., & Ma, Z. W. (1994). Kinetic Alfvén waves as a source of plasma transport at the dayside magnetopause. *Journal of Geophysical Research*, *99*, 17405–17411.
Louarn, P., Wahlund, J. E., Chust, T., et al. (1994). Observations of kinetic Alfvén waves by the Freja spacecraft. *Geophysical Research Letters*, *21*, 1847–1850.
Lundin, R., Haerendel, G., & Grahn, S. (1994). The Freja science mission. *Space Science Reviews*, *70*, 405–419.
Lysak, R. L., & Carlson, C. W. (1981). Effect of microscopic turbulence on magnetosphere-ionosphere coupling. *Geophysical Research Letters*, *8*, 269–272.
Lysak, R. L., & Dum, C. T. (1983). Dynamics of magnetosphere-ionosphere coupling including turbulent transport. *Journal of Geophysical Research*, *88*, 365–380.
Lysak, R. L., & Hudson, M. K. (1979). Coherent anomalous resistivity in the region of electrostatic shocks. *Geophysical Research Letters*, *6*, 661–663.
Lysak, R. L., & Hudson, M. K. (1987). Effect of double layers on magnetosphere-ionosphere coupling. *Laser Particle Beams*, *5*, 351–366.
Mölkki, A., Eriksson, A. I., Dovner, P. O., et al. (1993). A statistical survey of auroral solitary waves and weak double layers-1. Occurrence and net voltage. *Journal of Geophysical Research*, *98*, 15521–15530.
Mcllwain, C. E. (1960). Direct measurements of particles producing visible auroras. *Journal of Geophysical Research*, *65*, 2727–2747.
Mozer, F. S., Cattell, C. A., Hudson, M. K., et al. (1980). Satellite measurements and theories of low altitude auroral particle acceleration. *Space Science Reviews*, *27*, 155–213.
Mozer, F. S., Cattell, C. A., Temerin, M., et al. (1979). The dc and ac electric field, plasma density, plasma temperature, and field-aligned current experiments on the S3–3 satellite. *Journal of Geophysical Research*, *84*, 5875–5884.
Papadopoulos, K. (1977). A review of anomalous resistivity for the ionosphere. *Reviews of Geophysics*, *15*, 113–127.
Parker, E. N. (1958). Interaction of the solar wind with the geomagnetic field. *The Physics of Fluids*, *1*, 171–187.
Reiff, P. H., Collin, H. L., Craven, J. D., et al. (1988). Determination of auroral electrostatic potentials using high-and low-altitude particle distributions. *Journal of Geophysical Research*, *93*, 7441–7565.
Russell, C. T. (1995). A brief history of solar-terrestrial physics. In M. G. Kivelson & C. T. Russell (Eds.), *Introduction to space physics* (pp. 1–26). New York: Cambridge University Press.
Shukla, P. K., Rahman, H. D., & Sharma, R. P. (1982). Alfvén soliton in a low-beta plasma. *Journal of Plasma Physics*, *28*, 125–131.
Stasiewicz, K., Bellan, P., Chaston, C., et al. (2000a). Small scale Alfvénic structure in the aurora. *Space Science Reviews*, *92*, 423–533.
Stasiewicz, K., Gustafsson, G., Marklund, G., et al. (1997). Cavity resonators and Alfvén resonance cones observed on Freja. *Journal of Geophysical Research*, *102*, 2565–2575.
Stasiewicz, K., Holmgren, G., & Zanetti, L. (1998). Density depletions and current singularities observed by Freja. *Journal of Geophysical Research*, *103*, 4251–4260.
Stasiewicz, K., Khotyaintsev, Y., Berthomier, M., & Wahlund, J. E. (2000b). Identification of widespread turbulence of dispersive Alfvén waves. *Geophysical Research Letters*, *27*, 173–176.

Stasiewicz, K., Seyler, C. E., Mozer, F. S., et al. (2001). Magnetic bubbles and kinetic Alfvén waves in the high-latitude magnetopause boundary. *Journal of Geophysical Research*, *106*, A29503–29514.

Stewart, B. (1882). On the connexion between the state of the sun's surface and the horizontal intensity of the Earth's magnetism. *Proceedings of the Royal Society of London*, *34*, 406–409.

Temerin, M., Cerny, K., Lotko, W., & Mozer, F. S. (1982). Observations of double layers and solitary waves in the auroral plasma. *Physical Review Letters*, *48*, 175–1179.

Thompson, B. J., & Lysak, R. L. (1996). Electron acceleration by inertial Alfvén waves. *Journal of Geophysical Research*, *101*, 5359–5369.

Vaivads, A., Rönnmark, K., Oscarsson, T., & André, M. (1998). Heating of beam ions by ion acoustic waves. *Annales Geophysicae*, *16*, 403–412.

Vogt, J., & Haerendel, G. (1998). Reflection and transmission of Alfvén waves at the auroral acceleration region. *Geophysical Research Letters*, *25*, 277–280.

Volwerk, M., Louarn, P., Chust, T., et al. (1996). Solitary kinetic Alfvén waves-a study of the Poynting flux. *Journal of Geophysical Research*, *101*, 13335–13343.

Wahlund, J. E., Eriksson, A. I., Holback, B., et al. (1998). Broadband ELF plasma emission during auroral energiztion 1. Slow ion acoustic waves. *Journal of Geophysical Research*, *103*, 4343–4375.

Wahlund, J. E., Louarn, P., Chust, T., et al. (1994a). On ion-acoustic turbulence and the nonlinear evolution of kinetic Alfvén waves in aurora. *Geophysical Research Letters*, *21*, 1831–1834.

Wahlund, J. E., Louarn, P., Chust, T., et al. (1994b). Observations of ion acoustic fluctuations in the auroral topside ionosphere by the Frejia S/C. *Geophysical Research Letters*, *21*, 1835–1838.

Wolf, R. A. (1995). Magnetospheric configuration. In M. G. Kivelson & C. T. Russell (Eds.), *Introduction to space physics* (pp. 288–329). New York: Cambridge University Press.

Wu, C. S., & Lee, L. C. (1979). A theory of the terrestrial kilometric radiation. *The Astrophysical Journal*, *230*, 621–626.

Wu, D. J. (2003a). Model of nonlinear kinetic Alfvén waves with dissipation and acceleration of energetic electrons. *Physical Review E*, *67*, 027402.

Wu, D. J. (2003b). Dissipative solitary kinetic Alfvén waves and electron acceleration. *Physics of Plasmas*, *10*, 1364–1370.

Wu, D. J. (2010). Kinetic Alfvén waves and their applications in solar and space plasmas. *Progress in Physics*, *30*, 101–172.

Wu, D. J. (2012). *Kinetic Alfvén wave: Theory, experiment and application*. Beijing: Science Press.

Wu, D. J., & Chao, J. K. (2003). Auroral electron acceleration by dissipative solitary kinetic Alfvén waves. *Physics of Plasmas*, *10*, 3787–3789.

Wu, D. J., & Chao, J. K. (2004). Model of auroral electron acceleration by dissipative solitary kinetic Alfvén wave. *Journal of Geophysical Research*, *109*, A06211.

Wu, D. J., & Wang, D. Y. (1996). Solitary kinetic Alfvén waves on the ion-acoustic velocity branch in a low-β plasma. *Physics of Plasmas*, *3*, 4304–4306.

Wu, D. J., Huang, G. L., & Wang, D. Y. (1996a). Dipole density solitons and solitary dipole vortices in an inhomogeneous space plasma. *Physical Review Letters*, *77*, 4346–4349.

Wu, D. J., Huang, G. L., Wang, D. Y., & Fälthammar, C. G. (1996b). Solitary kinetic Alfvén waves in the two-fluid model. *Physics of Plasmas*, *3*, 2879–2884.

Wu, D. J., Wang, D. Y., & Fälthammar, C. G. (1995). An analytical solution of finite-amplitude solitary kinetic Alfvén waves. *Physics of Plasmas*, *2*, 4476–4481.

Wu, D. J., Wang, D. Y., & Huang, G. L. (1997). Two dimensional solitary kinetic Alfvén waves and dipole vortex structures. *Physics of Plasmas*, *4*, 611–617.

Yu, M. Y., & Shukla, P. K. (1978). Finite amplitude solitary Alfvén waves. *The Physics of Fluids*, *21*, 1457–1458.

Zabusky, N. J., & Kruskal, M. D. (1965). Interaction of "solitons" in a collisionless plasma and the recurrence of initial states. *Physical Review Letters*, *15*, 240–243.